Les Cahiers du GERAD ISSN: 0711–2440

Evacuation network design and planning under traffic congestion

A. Moreno, V. Bélanger, M. Cherkesly, M.-È. Rancourt

G–2024–55

Septembre 2024

La publication de ces rapports de recherche est rendue possible grâce au soutien de HEC Montréal, Polytechnique Montréal, Université McGill, Université du Québec à Montréal, ainsi que du Fonds de recherche du Québec – Nature et technologies.

Dépôt légal – Bibliothèque et Archives nationales du Québec, 2024
– Bibliothèque et Archives Canada, 2024

The publication of these research reports is made possible thanks to the support of HEC Montréal, Polytechnique Montréal, McGill University, Université du Québec à Montréal, as well as the Fonds de recherche du Québec – Nature et technologies.

Legal deposit – Bibliothèque et Archives nationales du Québec, 2024
– Library and Archives Canada, 2024

GERAD HEC Montréal
3000, chemin de la Côte-Sainte-Catherine
Montréal (Québec) Canada H3T 2A7

Tél. : 514 340-6053
Téléc. : 514 340-5665
info@gerad.ca
www.gerad.ca

Evacuation network design and planning under traffic congestion

Alfredo Moreno [a, b]

Valérie Bélanger [b]

Marilène Cherkesly [c, d]

Marie-Ève Rancourt [b]

[a] *Department of Industrial Engineering, Universidad del Norte, Barranquilla, 081007, Colombia*

[b] *Department of Logistics and Operations management, HEC Montréal, Montreal (Qc), Canada, H3T 2A7*

[c] *Département d'analytique, opérations et technologies de l'information, Université du Québec à Montréal, Montréal (Qc), Canada, H3C 3P8*

[d] *GERAD, Montréal (Qc), Canada, H3T 1J4*

arteagama@uninorte.edu.co
valerie.3.belanger@hec.ca
cherkesly.marilene@uqam.ca
marie-eve.rancourt@hec.ca

Septembre 2024
Les Cahiers du GERAD
G–2024–55

Abstract : Designing efficient evacuation networks is crucial for disaster preparedness, as poorly planned and managed evacuations can increase the time required for evacuees to reach safety zones or shelters, and potentially resulting in more casualties. Incorporating traffic considerations into evacuation network design and planning is essential to mitigate these risks. While some studies have estimated traffic congestion, few have integrated multiple aspects of evacuation planning, which is crucial for developing effective and realistic plans but leads to complex optimization problems. In this study, we propose and solve a mixed-integer programming model to address the Evacuation Network Design and Planning Problem under Traffic Congestion (ENDPPTC). Our model concurrently optimizes shelter locations, evacuation routes, and evacuee flows to minimize total evacuation time. Traffic congestion is modeled using a CTM-based formulation that accounts for time-varying road properties, multiple time periods, contraflow operations, and road segment capacities, ensuring a precise representation of traffic dynamics. To solve the ENDPPTC, we develop both exact and heuristic methods based on Benders decomposition. We also generate problem instances based on real-world network configurations to create representative and standardized benchmarks. Our computational results demonstrate that neglecting traffic congestion leads to inaccurate evacuation time estimates and significant delays, whereas incorporating contraflow operations significantly reduces total evacuation time.

Keywords : Evacuation planning, shelter network design, traffic management, Benders decomposition, mumanitarian logistics

Acknowledgements: This research was supported by Natural Resources Canada through the grant and contribution program. This research was also supported by the Natural Sciences and Engineering Research Council of Canada (NSERC), through the Discovery Grants Program, Grant 2017–05296, by GERAD, through the postdoctoral research grant, and by IVADO, through the Fundamental Research Program grant.

1 Introduction

Over the last decade, more than 3,800 natural disasters have been recorded globally (EM-DAT, 2022). The frequency and intensity of events such as floods, hurricanes, and wildfires have escalated during this period (Hsiao et al., 2021; Insani et al., 2022), causing billions in economic losses and affecting 1.51 billion individuals (EM-DAT, 2022). When human safety is threatened, the evacuation of a community, or part of a community, is often necessary (Kulshrestha et al., 2011; Bayram and Yaman, 2018a). Evacuations ensure the safety of populations through their prompt and efficient relocation to safer areas (Nunes et al., 2014). Notable instances include the evacuation of over one million individuals from southeast Louisiana during Hurricane Katrina in 2005 (Wolshon et al., 2006), the displacement of 88,000 residents during the 2016 Horse River fire in Fort McMurray (McGee, 2019), and the evacuation of more than 13,000 people following the 2020 breakup of the Athabasca River, which led to extensive flooding (Nafziger et al., 2021). Evacuations often pose significant logistical challenges, including road closures and restricted vehicle access (Wolshon et al., 2006; McGee, 2019), underscoring the critical need for well-prepared evacuation plans. In practice, closing some roads and directing traffic into desired routes can be used to control traffic and increase evacuation capacity (Wolshon et al., 2006).

Evacuation planning starts well before any imminent threat arises and involves several decisions. Three decisions are of utmost importance from a logistical perspective: locating shelters, establishing primary evacuation routes, and determining the flow of evacuees. First, shelter locations are strategically selected from potential safe sites, such as sports centers and hotels, that are situated outside threatened areas and equipped to provide temporary accommodation (Esposito Amideo et al., 2021). Second, safe evacuation routes are established considering the capacity of available roads. Finally, flow decisions determine the number of evacuees that travel on the roads to reach the shelters. Evacuation operations, however, trigger a massive, simultaneous movement of individuals towards roadways, leading to congestion and preventing evacuees from reaching safer locations quickly (Wolshon, 2001; White et al., 2008; Bayram and Yaman, 2018a). Consequently, it is crucial to consider the impact of traffic congestion when planning evacuations, ensuring that decisions accommodate the anticipated increase in road usage and facilitate a smoother evacuation process.

The Cell Transmission Model (CTM) is one of the most common approaches used to assess traffic congestion (Bayram, 2016). The CTM is a discretization of the hydrodynamic model of Lighthill and Whitham (1955), in which the traffic flow is treated as a fluid and formulations are based on the assumptions that there is a one-to-one relationship between speed and density, and traffic is conserved. CTM-based approaches include realistic traffic phenomena such as disturbance propagation, non-linearity between speed–density and travel time–density, and the creation of shockwaves (Ziliaskopoulos, 2000). Despite these advantages, the complexity of the optimization models underlying CTM increases rapidly with network size, leading to significant computational challenges (Zheng and Chiu, 2011). To address these challenges, heuristics and network flow-based algorithms have been developed to efficiently manage realistic-sized networks (Kimms and Maassen, 2012a,b; Bish and Sherali, 2013; Zheng et al., 2015; Bayram and Yaman, 2024).

Although traffic congestion has been considered in the context of evacuation planning, few studies take into account shelter location, contraflow operations, and the dynamic nature of evacuations simultaneously. Incorporating these elements is crucial to ensure effective and realistic evacuation plans. First, shelter location decisions are critical as they influence the routes evacuees take from threatened areas to shelters, directly impacting traffic congestion (He et al., 2018). Contraflow operations, which involve reversing the direction of traffic lanes to temporarily expand roadway capacity, can also be employed to reduce congestion and influence evacuation duration (Esposito Amideo et al., 2021; Kim et al., 2008). Additionally, evacuations are inherently dynamic, with varying conditions that can alter the parameters of the problem over time. Therefore, dynamic models that account for these temporal variations offer a more accurate representation of evacuations compared to static models (Bayram, 2016; Li et al., 2019).

In this paper, we consider the Evacuation Network Design and Planning Problem under Traffic Congestion (ENDPPTC), which aims to select shelter locations, establish evacuation routes, including the number of lanes to be used in each direction (i.e., considering contraflow operations), and defining the flow of evacuees on road segments. The goal is to minimize the total evacuation time, defined as the sum of the evacuation times for all evacuees from the beginning of the time horizon to their arrival at a safe location, including delays due to traffic congestion. We incorporate traffic congestion using a CTM-based formulation that captures time-variant road segment properties, multiple periods, and road capacities to ensure an accurate representation of traffic phenomena. Our focus is on mass self-evacuation or car-based evacuation, where people use their own vehicles to drive to the shelters. Those without a private vehicle may rely on alternatives, such as riding with friends or neighbors (Dulebenets et al., 2019). Our main contributions include employing a more precise traffic model to address congestion in evacuation network design, while also integrating traffic management. These advancements result in complex models, prompting the development of a Benders decomposition (BD) approach to effectively solve realistic instances. We also provide diverse and realistic instances to facilitate the testing of methods for designing evacuation networks.

The remainder of the paper is organized as follows. Section 2 reviews the relevant background literature. Section 3 describes the ENDPPTC and presents the mathematical formulation. Section 4 provides the solution approaches. Section 5 describes the instances and discusses the computational results. We close with concluding remarks in Section 6.

2 Literature review

Evacuation planning and traffic management play a critical role in ensuring the safe and timely evacuation of the vulnerable population (Bayram, 2016). In the planning phase, evacuation network design focuses on selecting shelter locations, managing capacity, and determining evacuation routes based on the transportation network. Once the evacuation is triggered in the response phase, evacuees will move through the network, and the flow of evacuees on each road segment will influence travel times: higher flows lead to increased congestion, thereby prolonging the time to reach safety. Most studies have only focused on either evacuation network design (Coutinho-Rodrigues et al., 2012; Hadas and Laor, 2013; Sheu and Pan, 2014; Üster et al., 2018; Esposito Amideo et al., 2021) or traffic management and modelling in the context of evacuation (Yao et al., 2009; Ng et al., 2010; Kimms and Maassen, 2012a,b; Lim et al., 2015; Yan et al., 2018; Li et al., 2019). Only a few studies have considered both simultaneously.

In this section, we focus on OR optimization models and methods that are closely related to the ENDPPTC, i.e., those that tackle network- and traffic-related decisions jointly. We then position our study within the existing literature. We refer the reader to Murray-Tuite and Wolshon (2013), Bayram (2016), Esposito Amideo et al. (2019), and Dönmez et al. (2021) for a more comprehensive review of shelter location and evacuation planning. Finally, it is important to note that studies that consider traffic congestion via micro-simulation (Jha et al., 2004; Alam and Habib, 2021b,a) and empirical studies related to evacuation planning (Wong et al., 2018; Christianson and McGee, 2019; Hessami et al., 2020) are beyond the scope of this review.

2.1 Evacuation network design under traffic congestion

Sherali et al. (1991) are the first to consider traffic congestion in evacuation network design planning with the goal of minimizing the total evacuation time. The authors propose a single period nonlinear mixed-integer programming problem with congestion-related travel times. In particular, the problem considers shelter location and route definition decisions and is solved using a heuristic and an exact implicit enumeration algorithm based on Benders decomposition. The authors use the Bureau of Public Roads (BPR) function to approximate the impact of traffic congestion. The BPR function expresses the relationship between travel time and traffic volume on a link based on parameters defined by the

United States Department of Commerce (Bureau of Public Roads, 1964). The proposed approach is tested using data from the Virginia Beach network. Similarly, Kongsomsaksakul et al. (2005) propose a model that uses the BPR function to approximate traffic, but in a bilevel optimization framework. The upper level is formulated as a shelter location problem whereas the lower level is defined as a combined distribution and assignment model that determines the flow of evacuees in the network under traffic congestion. The problem is solved using a genetic algorithm and tested considering a hypothetical flood scenario in the city of Logan, Utah.

These two models consider a deterministic problem, where the number of evacuees and the availability of roads and shelters are known a priori. Kulshrestha et al. (2011) introduce the uncertainty related to the number of people to evacuate into the problem using a bilevel robust optimization approach. The model determines shelter locations, selects routes and determines the flow of evacuees that minimize the total cost of establishing and operating shelters while taking into account a predetermined time limit to perform evacuation operations. The authors again use a BPR function to consider traffic congestion and solve the problem using a cutting plane algorithm. The model is tested using data from the city of Sioux Falls under a hypothetical disaster. In addition to demand uncertainty, Li et al. (2012) also consider the availability of shelters in a stochastic bilevel framework. The proposed model aims to minimize the weighted sum of the expected unmet demand, i.e., people who could not find shelters, and the total evacuation time. The upper level considers shelter location-allocation decisions, while the lower level determines the flow of evacuees. The problem is solved with a Lagrangian relaxation-based heuristic, and tested using historical hurricane data from the state of North Carolina.

Bayram et al. (2015) develop a nonlinear integer programming model that locates shelters and assigns evacuees to the closest shelter and to the shortest path within a tolerance distance range, minimizing the total evacuation time. The BPR function is used to model flow-dependent travel time on road segments. They linearized the problem using second-order cone programming techniques. The model is tested using data from the Istanbul Metropolitan Municipality and the Japan International Cooperation Agency for earthquake preparedness. Bayram and Yaman (2018a) extend the model proposed in Bayram et al. (2015) introducing uncertainty in the number of evacuees and in the availability of roads and shelters, leading to a scenario-based two-stage stochastic model. In this case, twelve earthquake scenarios were considered based on various magnitudes and severity levels. Bayram and Yaman (2018b) then developed an exact algorithm based on Benders decomposition to solve the two-stage stochastic model with a large number of scenarios.

In addition to main decisions, such as shelter location and flow definition, He et al. (2018) also integrate contraflow operations in their optimization model. They consider traffic congestion via the earliest arrival flow (EAF) model, as an approximation of the CTM, and aim to minimize the total evacuation time. A Benders decomposition algorithm is developed to solve the problem on data from the Dallas-Fort Worth Metropolitan Area. Finally, Afkham et al. (2022) consider traffic via a BPR function and proposed a bilevel model to minimize the total evacuation time. They also consider that some roads could be equipped for contraflow. The upper level decides on the selection of shelters and on the roads to be equipped. The lower level determines the flow of evacuees. They propose a Benders decomposition algorithm to solve the problem.

Table 1 summarizes the studies on network design under traffic congestion and positions our study within the related literature. It presents the objective function, targeting either evacuation time, cost, or coverage (Cov.), and highlights the main decisions of each optimization model. Location (Loc.) indicates whether or not shelter location is treated as a decision variable in the model. Flow Determination (Flow det.) identifies whether or not the model determines the number of evacuees assigned to each road segment. Path Selection (Path sel.) and Route Definition (Route def.) both relate to how evacuation routes are established, specifically which road segments are used during the evacuation. Path Selection refers to cases where routes are chosen from a predefined set, while Route Definition applies when evacuation routes and the flow of evacuees on each segment are determined simultaneously. Lastly, Link Capacity (Link Cap.) denotes whether or not the model includes decisions on the

number of lanes available on each road segment. The table also indicates whether the optimization model is multi-period and whether it considers contraflow operations. Additionally, it reports the approach used to approximate traffic congestion and outlines the solution methods employed to solve the proposed optimization models.

Table 1: Reviewed studies integrating shelter location decisions and traffic congestion

	Objective			Main decisions					Characteristics			
Reference	Time	Cost	Cov.	Loc.	Flow det.	Path sel.	Route def.	Link cap.	Multi-period	Contra-flow	Traffic congestion	Solution approaches
Sherali et al. (1991)	✓			✓	✓		✓				BRP	BD, heuristic
Kongsomsaksakul et al. (2005)	✓			✓	✓	✓					BRP	Genetic algorithm
Kulshrestha et al. (2011)		✓		✓	✓		✓				BRP	Cutting plane algorithm
Li et al. (2012)	✓		✓	✓	✓				*		BRP	Lagrangian relaxation
Bayram et al. (2015)	✓			✓	✓	✓					BRP	Commercial solver
Bayram and Yaman (2018a)	✓			✓	✓	✓					BRP	Commercial solver
Bayram and Yaman (2018b)	✓			✓	✓	✓					BRP	BD
He et al. (2018)	✓			✓	✓		✓		✓	✓	EAF	BD
Afkham et al. (2022)	✓			✓	✓		✓		*	✓	BRP	BD
This paper	✓			✓	✓		✓	✓	✓	✓	CTM	BD, heuristic

* The entire evacuation period is divided into independent time intervals.

2.2 Positioning and contributions of our paper

In this section, we position our study within the existing literature by examining how our approach compares to previous research on evacuation network design under traffic congestion. We also highlight the contributions of our work.

Several approaches have been employed to establish evacuation routes and determine the flow of evacuees. Li et al. (2012) defined the flow between threatened areas and shelters, assuming that only one path is available for evacuation between each pair of areas and shelters. Other studies have explored either path selection (Kongsomsaksakul et al., 2005; Bayram et al., 2015; Bayram and Yaman, 2018b,a) or route definition (Sherali et al., 1991; Kulshrestha et al., 2011; He et al., 2018; Afkham et al., 2022). However, none of the reviewed studies explicitly consider road segment capacity, which is particularly relevant when implementing traffic management strategies such as contraflow operations. The capacity of a road segment depends on the number of lanes designated for contraflow operations and the number of lanes reserved for inbound traffic, such as for police and rescue teams entering threatened areas. Although He et al. (2018) and Afkham et al. (2022) consider contraflow operations as a means to reduce traffic congestion, they do not account for partial inbound flow, meaning all lanes are dedicated to outbound traffic. Moreover, Afkham et al. (2022) assumed a predefined capacity on each link as an input for the BPR function, without considering the potential to increase road segment capacities through contraflow operations, as we do.

Traffic congestion has been considered mostly through the BPR function. No studies consider traffic congestion along with shelter location using more sophisticated and more precise approximation of traffic, using CTM-based approaches for instance. With the BPR function, the travel time on the links is expressed as a non-linear function of the traffic volume, resulting in non-linear optimization models. The linearization of the models is usually done using piecewise linear approximations. Furthermore, He et al. (2018) used an Earliest Arrival Flow (EAF) model to incorporate traffic congestion. The EAF is a link-based approximation of the cell-transmission model (CTM) with time-invariant cell

properties (Zheng et al., 2015). In general, BPR and EAF-based formulations are easier to solve than CTM-based formulations. However, according to He et al. (2018), the EAF model is not able to capture detailed traffic dynamics and was developed for cases with time-invariant link properties. In addition, the BPR function is a link exit function that does not directly consider different traffic phenomena such as disturbance propagation and the creation of shockwaves, which are common in congested networks (Ziliaskopoulos, 2000; Waller and Ziliaskopoulos, 2006). Therefore, CTM-based formulations are expected to provide better estimations of traffic congestion than BPR and EAF-based formulations.

Most of the studies ignored the dynamic nature of evacuation operations. He et al. (2018) is the only work integrating shelter location and traffic congestion using a dynamic setting, i.e., defining the flow of evacuees over multiple periods. Their formulation is based on the assumption that link capacities are time-invariant. In addition, although Li et al. (2012) and Afkham et al. (2022) divided the evacuation period into smaller time intervals, they solved the problem for each sub-period independently, without considering a multi-period framework. Dynamic models can provide better estimations of the impact of traffic on congested networks (Bayram, 2016).

In this paper, we advance the literature by exploring evacuation network design and planning under traffic congestion in a dynamic setting, with our contribution being threefold. First, we define and formulate the Evacuation Network Design and Planning Problem under Traffic Congestion (ENDPPTC). Our mathematical formulation integrates a state-of-the-art traffic model, the CTM, with shelter location decisions, contraflow operations, time-variant road segment properties, multiple periods, and road capacities. These features, which have not been considered simultaneously before, significantly influence the time required for a safe evacuation. However, this integration results in a formulation that is challenging to solve for real-world instances using commercial solvers or existing methods developed for other variants of evacuation planning problems. As a second contribution, we develop both exact and heuristic solution methods based on Benders decomposition, an approach that has been successfully applied in similar contexts (Rahmaniani et al., 2017; Bayram and Yaman, 2018b; He et al., 2018; Afkham et al., 2022; Xu and Nair, 2024). Third, we generate problem instances with varying topologies and network sizes, inspired by real-world configurations, and conduct extensive computational experiments. Through these experiments, we analyze the solutions provided by our proposed formulations and offer practical insights based on our results.

3 Problem description and mathematical model

In this section, we describe the problem under study, introduce the mathematical notation, and present the mathematical formulation. For summary purposes, a complete list of the mathematical notation is provided in Appendix A.

3.1 Problem description and mathematical notation

The Evacuation Network Design and Planning Problem under Traffic Congestion (ENDPPTC) involves different decisions: (i) the location of shelters, (ii) the evacuation routes, (iii) the number of lanes on the roads that are used during the evacuation (including contraflow operations), and (iv) the flow of evacuees on the roads during the evacuation. The objective is to minimize the total evacuation time, i.e., the total travel time spent by evacuees to reach shelters, including delays and waiting times due to traffic congestion. We assume that all evacuees are ready to evacuate at the beginning of the time horizon. Additionally, we assume that evacuees follow the routing guidance and instructions of local authorities or are influenced in their route choice by security forces and police traffic guidance (Goerigk et al., 2014). In the following, we first define the ENDPPTC on the directed graph G representing the network without traffic congestion. Then, we explain how this graph is modified to incorporate traffic congestion using a cell-representation graph G^{τ}.

3.1.1 Directed graph G without traffic congestion

The ENDPPTC can be defined on a directed graph $G = (\mathcal{V}, \mathcal{E})$, in which $\mathcal{V}$ is the set of nodes and $\mathcal{E}$ is the set of directed links. The node set $\mathcal{V} = \mathcal{V}^{\mathtt{s}} \cup \mathcal{V}^{\mathtt{d}} \cup \mathcal{V}^{\mathtt{u}} \cup \{p\}$ comprises a set of source nodes $\mathcal{V}^{\mathtt{s}}$ (e.g., population points, households, meeting points, facilities), destination nodes $\mathcal{V}^{\mathtt{d}}$ (e.g., shelters, safe zones, exit points), intersection nodes $\mathcal{V}^{\mathtt{u}}$ (i.e., road intersections) and a sink node p, with $\mathcal{V}^{\mathtt{s}} \cap \mathcal{V}^{\mathtt{d}} = \emptyset$. The set of directed links $\mathcal{E}$ includes one link from each destination node $\mathcal{V}^{\mathtt{d}}$ to the sink node p denoted as $\mathcal{E}^p$ and the set of roads denoted as $\mathcal{E} \setminus \mathcal{E}^p$. Figure 1 presents an example of a graph G with three source nodes, two destination nodes, two intersection nodes, and nine roads represented with 18 directed links.

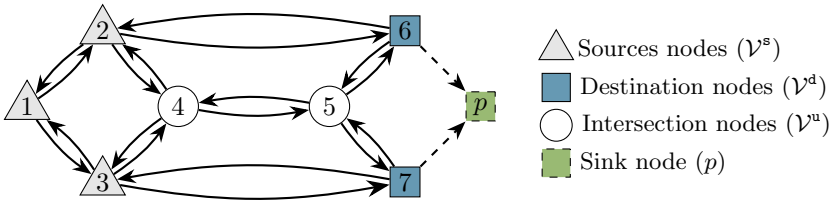

Figure 1: Example of a graph G

Each source node $i \in \mathcal{V}^{\mathtt{s}}$ has a demand (b_i), measured in number of vehicles, to be evacuated. A shelter with a limited capacity K_i of number of vehicles that it can receive can be opened or not at each destination node $i \in \mathcal{V}^{\mathtt{d}}$. In addition, a shelter can only be opened if at least $m^{\mathtt{d}}$ vehicles reach it. This consideration helps to enhance staff deployment and management by preventing too low utilization rates of available resources, including shelter facilities, staff, beds, food, and other essentials. While there is no cost to open (use) a shelter, at most $\mathtt{K}$ shelters can be opened due to the limited resources available for setting up and managing shelters.

To reach shelters, evacuees have to travel on a road-network. Each road goes from one node $i \in \mathcal{V} \setminus p$ to another node $j \in \mathcal{V} \setminus p$ and is represented by exactly two directed links in $\mathcal{E} \setminus \mathcal{E}^p$, i.e., implying that it can be used in both directions. Each link $e \in \mathcal{E} \setminus \mathcal{E}^p$ has a length in miles (μ_e) and a number of lanes (f_e) that can be used for evacuation. Contraflow operations are allowed, i.e., some lanes can be used in the opposite direction to facilitate the evacuation. However, at most $f_e^{\mathtt{M}}$ lanes of link $e \in \mathcal{E} \setminus \mathcal{E}^p$ can be used in contraflow and we impose a maximum total number E of links with contraflow operations. This is due to the resources required to deploy the contraflow operations, e.g., limited staff (police officers) needed to control the new flow direction. In addition, this allows to consider that some lanes need to remain available in their initial direction for inbound flow (police, National Guard, rescue teams, etc.) into threatened areas (Wolshon, 2001). Each link $e \in \mathcal{E} \setminus \mathcal{E}^p$ is also associated with three traffic-related parameters: its free-flow capacity representing the maximum number of vehicles that can pass per hour without traffic congestion (q_e), a free-flow speed representing the speed without traffic congestion in miles per hour (v_e), and its free-flow travel time in seconds which is computed as its length divided its free-flow speed and reported in seconds, that is, $t_e = \mu_e / v_e \cdot 3600$. In practice, using a link requires resources to be deployed such as policemen to guide the people, or signs. Therefore, a link $e \in \mathcal{E} \setminus \mathcal{E}^p$ can only be used if at least $m^{\mathtt{e}}$ vehicles traverse it.

3.1.2 Cell-representation graph G^τ including traffic congestion

In the ENDPPTC, all the demand must be evacuated within a predefined time horizon T^τ for which each period $t \in T^\tau$ has a time step τ. A better estimation of the traffic congestion is obtained with lower values of τ, but this increases the complexity of the problem. The travel time on links depend on the congestion induced by the flow of vehicles. Travel times are usually positive and monotonically increasing functions of traffic flow, meaning that higher traffic volumes result in longer travel times. To model traffic congestion, we use the Cell Transmission Model (CTM) approach as proposed by Daganzo (1994, 1995). The CTM is a discretization of the differential equations of

the Lighthill–Whitham–Richards (LWR) hydrodynamic theory of traffic flow (Lighthill and Whitham, 1955; Richards, 1956), in which the traffic flow is treated as a fluid, and there are two basic assumptions: there is a one-to-one relationship between speed and density, and traffic is conserved. The general idea of the CTM is to convert roads (links) into equal-sized segments, called cells, each of which has a length that is equal to the distance that can be traveled during the predefined time step τ at the free-flow speed, i.e., the travel speed without traffic (Bayram, 2016). Congestion occurs when the flow in one cell cannot be propagated to the next, i.e., when vehicles must wait in a cell for one or multiple periods before going to the next. In the following, we describe how the directed graph G is transformed into the cell-representation graph G^τ to consider traffic congestion using the CTM approach.

Each source node $i \in \mathcal{V}^{\mathtt{s}}$ is represented by a source cell, and the set of source cells is denoted by $\mathcal{C}^{\mathtt{s}}$. Each destination node $i \in \mathcal{V}^{\mathtt{d}}$ is represented by a destination cell, and the set of destination cells is denoted by $\mathcal{C}^{\mathtt{d}}$. The sink node p is represented by a sink cell also denoted by p. Each link $e \in \mathcal{E}$ is associated with a set of cells $\mathcal{C}_e$. Therefore, the set of cells is defined as $\mathcal{C} = \mathcal{C}^{\mathtt{s}} \cup \mathcal{C}^{\mathtt{d}} \cup \{p\} \cup_{e \in \mathcal{E}} \mathcal{C}_e$. In the cell-representation graph G^τ, each cell is connected with a directed arc to its successor and predecessor cells. For each cell $j \in \mathcal{C}$, we denote by Γ_j and Γ_j^{-1} its set of successor and predecessor cells, respectively. Figure 2 illustrates the cell-representation graph G^τ of the graph G presented in Figure 1. The graph contains three source cells ($\mathcal{C}^{\mathtt{s}} = \{1, 2, 3\}$), two destination cells ($\mathcal{C}^{\mathtt{d}} = \{4, 5\}$), and 46 cells associated with links in graph G. As an example, the link $(2, 4)$ in the directed graph G is represented with the set of cells $\{8, 9, 10, 11\}$ in the cell-representation graph G^τ. In addition, for cell 8 in graph G^τ, its set of successor cells is defined as $\Gamma_8 = \{9\}$, while its set of predecessor cells is defined as $\Gamma_8^{-1} = \{2, 7, 45\}$.

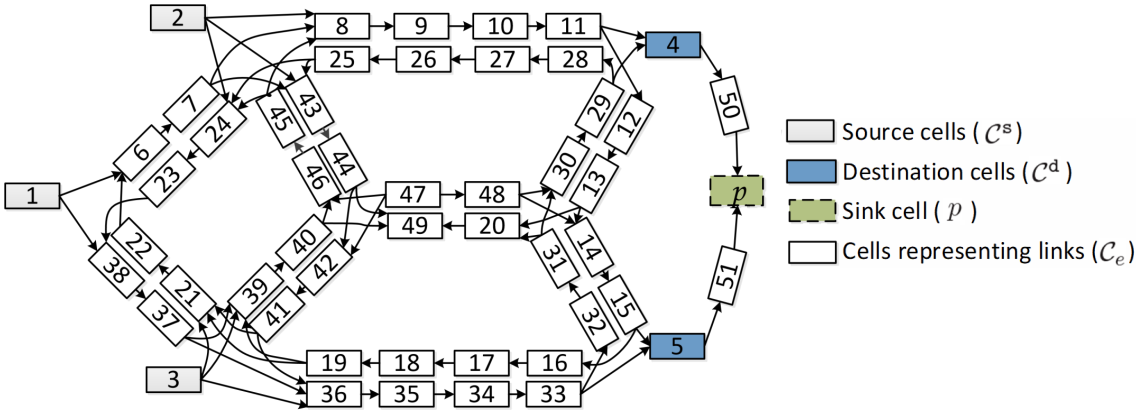

Figure 2: Example of a cell-representation graph G^τ

Each link $e \in \mathcal{E}$ is divided into ℓ_e cells ($|\mathcal{C}_e| = \ell_e$), where $\ell_e = \lceil t_e/\tau \rceil$, that is, the number of cells is computed as the free-flow travel time of edge e divided by the time step and rounded up to the nearest integer. Note that $\ell_e = 1$ for all $e \in \mathcal{E}^p$. In addition, the length in miles associated with each cell $\mathcal{C}_e, e \in \mathcal{E} \setminus \mathcal{E}^p$, denoted by d_e, is computed as $d_e = (\tau/3600)v_e$ and represents the distance that a vehicle can travel during a time step τ according to the free-flow speed of its associated link.

A parameter $0 \leq \delta \leq 1$ represents the ratio between the free-flow speed and the backward wave speed. A value closer to zero implies that there is more traffic which is propagated backwards in the cells. Therefore, the flow propagation between two cells at any time period $t \in T^\tau$ is bounded by i) the maximum number of vehicles that can be accommodated in cell $i \in \mathcal{C}_e, e \in \mathcal{E} \setminus \mathcal{E}^p$ given l lanes in operation (N_{ilt}), and ii) the maximum number of vehicles that can flow into or out (pass in or out) of cell $i \in \mathcal{C}_e, e \in \mathcal{E} \setminus \mathcal{E}^p$ given l lanes in operation (Q_{ilt}). We define $N_{ilt} = l\kappa d_e, \forall i \in \mathcal{C}_e, e \in \mathcal{E} \setminus \mathcal{E}^p$, where κ denotes the traffic jam density, i.e., the number of vehicles per mile per lane when traffic flow stops completely. We also compute $Q_{ilt} = l(\tau/3600)q_e, \forall i \in \mathcal{C}_e, e \in \mathcal{E} \setminus \mathcal{E}^p$.

3.2 Mathematical model

We model the ENDPPTC as a mixed-integer linear programming problem. Our model is adapted from the linear programming formulation proposed by Ziliaskopoulos (2000), which is a CTM-based flow model that considers evacuation planning and traffic congestion. In the ENDPPTC, the model is adapted to consider additional decisions related to shelter location, route definition, and link capacities, including contraflow operations.

The additional following notation is necessary to model the ENDPPTC. In the directed graph, each road is represented by exactly two directed links in $\mathcal{E} \setminus \mathcal{E}^p$. Therefore, for each pair of links $e, e' \in \mathcal{E} \setminus \mathcal{E}^p$, we define $g_{ee'}$ as a binary parameter equal to one if links e and e' represent the road in opposite directions, and 0 otherwise. We define $\mathcal{L}_e$ as the set of lanes that can be used on a given road in the same direction. For link $e \in \mathcal{E} \setminus \mathcal{E}^p$, given $e' \in \mathcal{E} \setminus \mathcal{E}^p$ such that $g_{ee'} = 1$, the number of lanes than can be used in the same direction is equal to $f_e + f^{\mathtt{M}}_{e'}$. Therefore, $\mathcal{L}_e = \{1, ..., f_e + f^{\mathtt{M}}_{e'}\}$, $\forall e, e' \in \mathcal{E} \setminus \mathcal{E}^p$ such that $g_{ee'} = 1$. We also define n_{ji} as a binary parameter equal to one if node $i \in \mathcal{V} \setminus \mathcal{V}^{\mathtt{u}}$ in graph G is represented by cell $j \in \mathcal{C} \setminus \cup_{e \in \mathcal{E}} \mathcal{C}_e$ in the cell-representation graph G^τ, and 0 otherwise.

The ENDPPTC can then be modeled using four sets of variables. First, for every destination node $i \in \mathcal{V}^{\mathtt{d}}$, we define Z_i as a binary variable equal to one if a shelter is opened at destination node i, and 0 otherwise. Second, for every directed link $e \in \mathcal{E} \setminus \mathcal{E}^p$, we define L_{le} as a binary variable equal to one if $l \in \mathcal{L}_e$ lanes are used during the evacuation, and 0 otherwise. Third, for every cell $j \in \mathcal{C}$ and period $t \in T^\tau$, we define X_{jt} as a continuous variable representing the number of vehicles in cell j at period t. Finally, for each pair of connected cells $j \in \mathcal{C}, k \in \Gamma_j$, we define Y_{jkt} as a continuous variable representing the number of vehicles moving from cell j to cell k at period $t \in T^\tau$. Using these variables, the ENDPPTC can be modeled as follows:

$$\text{(ENDPPTC)} \quad \min \quad \sum_{j \in \mathcal{C} \setminus \{p\}} \sum_{t \in T^\tau} \tau X_{jt}, \tag{1a}$$

$$\text{s.t.} \quad X_{j1} = b_i + X_{j0} - \sum_{k \in \Gamma_j} Y_{jk0}, \quad \forall\, j \in \mathcal{C}^{\mathtt{s}}, i \in \mathcal{V}^{\mathtt{s}} : n_{ji} = 1, \tag{1b}$$

$$X_{jt} = X_{j(t-1)} - \sum_{k \in \Gamma_j} Y_{jk(t-1)}, \quad \forall\, j \in \mathcal{C}^{\mathtt{s}}, t \in T^\tau : t > 1, \tag{1c}$$

$$X_{pt} = X_{p(t-1)} + \sum_{k \in \Gamma_p^{-1}} Y_{kp(t-1)}, \quad \forall\, t \in T^\tau, \tag{1d}$$

$$X_{jt} = X_{j(t-1)} + \sum_{k \in \Gamma_j^{-1}} Y_{kj(t-1)} - \sum_{k \in \Gamma_j} Y_{jk(t-1)}, \quad \forall\, j \in \mathcal{C} \setminus \{\mathcal{C}^{\mathtt{s}} \cup \{p\}\}, t \in T^\tau, \tag{1e}$$

$$\sum_{k \in \Gamma_j} Y_{jkt} \leq X_{jt}, \quad \forall\, j \in \mathcal{C} \setminus \{p\}, t \in T^\tau, \tag{1f}$$

$$\sum_{k \in \Gamma_j} Y_{jkt} \leq \sum_{l \in \mathcal{L}_e} Q_{jlt} L_{le}, \quad \forall\, j \in \mathcal{C}_e, e \in \mathcal{E} \setminus \mathcal{E}^p, t \in T^\tau, \tag{1g}$$

$$\sum_{j \in \Gamma_k^{-1}} Y_{jkt} \leq \sum_{l \in \mathcal{L}_e} Q_{klt} L_{le}, \quad \forall\, k \in \mathcal{C}_e, e \in \mathcal{E} \setminus \mathcal{E}^p, t \in T^\tau, \tag{1h}$$

$$\sum_{j \in \Gamma_k^{-1}} Y_{jkt} \leq \sum_{l \in \mathcal{L}_e} \delta N_{klt} L_{le} - \delta X_{kt}, \quad \forall\, k \in \mathcal{C}_e, e \in \mathcal{E} \setminus \mathcal{E}^p, t \in T^\tau, \tag{1i}$$

$$\sum_{t \in T^\tau} Y_{jpt} \leq K_i Z_i, \quad \forall\, j \in \mathcal{C}^{\mathtt{d}}, i \in \mathcal{V}^{\mathtt{d}} : n_{ji} = 1, \tag{1j}$$

$$\sum_{t \in T^\tau} \sum_{k \in \Gamma_j^{-1}} Y_{kjt} \geq m^{\mathtt{e}} \sum_{l \in \mathcal{L}_e} L_{le}, \quad \forall\, j \in \mathcal{C}_e, e \in \mathcal{E} \setminus \mathcal{E}^p, \tag{1k}$$

$$\sum_{t \in T^\tau} Y_{jpt} \geq m^{\mathtt{d}} Z_i, \quad \forall\, j \in \mathcal{C}^{\mathtt{d}}, i \in \mathcal{V}^{\mathtt{d}} : n_{ji} = 1, \tag{1l}$$

$$\sum_{i \in \mathcal{V}^{\mathrm{d}}} Z_i \leq \mathtt{K}, \tag{1m}$$

$$\sum_{l \in \mathcal{L}_e} L_{le} + \sum_{l \in \mathcal{L}_{e'}} L_{le'} \leq 1, \quad \forall\, e, e' \in \mathcal{E} \setminus \mathcal{E}^p : g_{ee'} = 1, \tag{1n}$$

$$\sum_{l \in \mathcal{L}_e} l L_{le} \leq f_e + f^{\mathtt{M}}_{e'}, \quad \forall\, e, e' \in \mathcal{E} \setminus \mathcal{E}^p : g_{ee'} = 1, \tag{1o}$$

$$\sum_{e \in \mathcal{E} \setminus \mathcal{E}^p} \sum_{l \in \mathcal{L}_e : l > f_e} L_{le} \leq E, \tag{1p}$$

$$X_{j|T^\tau|} = 0, \quad \forall\, j \in \mathcal{C} \setminus \{p\}, \tag{1q}$$

$$X_{jt} \geq 0, \quad \forall\, j \in \mathcal{C}, t \in T^\tau, \tag{1r}$$

$$Y_{jkt} \geq 0, \quad \forall\, j \in \mathcal{C}, k \in \Gamma_j, t \in T^\tau, \tag{1s}$$

$$Z_i \in \{0,1\}, \quad \forall\, i \in \mathcal{V}^{\mathrm{d}}, \tag{1t}$$

$$L_{le} \in \{0,1\}, \quad \forall\, l \in \mathcal{L}_e, e \in \mathcal{E} \setminus \mathcal{E}^p. \tag{1u}$$

The objective function (1a) minimizes the total evacuation time, i.e., the sum of the time required for all vehicles to reach the shelters. Constraints (1b) and (1c) define the cell-mass conservation for the source cells at period $t = 1$ and $t > 1$, respectively. That is, at period $t = 1$, the number of vehicles at a given source cell is equal to its demand. At period t, such that $t > 1$, the number of vehicles at a given source cell is equal to the number of vehicles that were at the source cell at period $t - 1$ by removing those that left to another cell at period $t - 1$. X_{j0} and Y_{jk0} represent the initial state of the system. Constraints (1d) define the cell-mass conservation for the sink cell p, i.e., the number of vehicles at the sink cell at period t is equal to the number of vehicles that were at the sink cell at period $t - 1$ added to those that arrived at the sink cell at period t. Similarly, constraints (1e) define the cell-mass conservation for all the other cells. Constraints (1f) state that the flow between cells j and k is bounded by the number of vehicles at the starting cell j. Similarly, constraints (1g) and (1h) state that the flow between cells j and k is bounded by the maximum flow that can flow out of the starting cell j and into the ending cell k, respectively, according to the number of lanes in operation. Constraints (1i) define that the flow between cells is bounded by the cell's remaining capacity which is affected by the ratio between its free-flow speed and its backward wave speed (δ) as in the literature (Ziliaskopoulos, 2000). That is, for a given cell $i \in \mathcal{C}_e, e \in \mathcal{E} \setminus \mathcal{E}^p$ at a given time period $t \in T^\tau$, it corresponds to the maximum number of vehicles that can be accommodated in a given cell minus the number of vehicles that are already in the cell, which is computed as $\delta(\sum_{l \in \mathcal{L}_e} N_{ilt} L_{le} - X_{it})$. Constraints (1j) limit the number of vehicles that can be evacuated to shelters. Constraints (1k) and (1l) establish the minimum flow on links and shelters to consider their operation. Constraint (1m) limits the number of shelters that can be opened. Constraints (1n) force the evacuation flow to only one direction for a given road segment. Constraints (1o) limit the number of lanes that can be used during evacuation operations to the number of available lanes, including the contraflow operations. Constraints (1p) set a limit on the number of links with contraflow operations. A giving link $e \in \mathcal{E} \setminus \mathcal{E}^p$ uses lanes in contraflow if the number of used lanes is higher than f_e. Constraints (1q) force the evacuation of all vehicles to the sink cell. Finally, constraints (1r) and (1u) establish the domain of decision variables.

4 Branch-and-Benders-cut algorithm to solve the ENDPPTC

It is important to develop specialized solution methods to solve the ENDPPTC due to the complexity of the problem. In the ENDPPTC, the problem can be decomposed to reduce its complexity using Benders decomposition. Furthermore, the impact of traffic congestion on evacuation time can be more precisely estimated when using shorter time periods, i.e., smaller values of τ. However, this leads to an increase in the number of variables and constraints, thus further complicating the model. In this section, we present an exact Branch-and-Benders-cut (BBC) algorithm to solve the ENDPPTC (Section 4.1). We also propose enhancement strategies to speed up our BBC algorithm (Section 4.2).

Additionally, in Appendix D we present an algorithm developed to solve the subproblem heuristically, which results in a matheuristic BBC. The matheuristic BBC is used to find feasible solutions, particularly for instances with small τ values.

4.1 Branch-and-Benders-cut algorithm

Benders decomposition is a variable-partitioning technique to efficiently solve complex problems (Benders, 1962; Rahmaniani et al., 2017). In our Benders decomposition approach to solve the ENDPPTC, the problem is decomposed in a master problem (MP) and a subproblem (SP). The MP considers only the binary variables, i.e., shelter location and lanes to be used during the evacuation. The SP determines the flow of evacuees on the different links during the evacuation considering the MP solution. In the classical Benders decomposition, the MP and the subproblem are solved iteratively (starting with the MP). At each iteration, violated (optimality or feasibility) Benders cuts derived from the SP are added to the MP. This process is repeated until a stopping criterion is reached (usually a running time limit or a predefined optimality gap). The optimality gap can be calculated at each iteration. The objective function of the MP gives a valid lower bound, while feasible SPs provide valid upper bounds for the original problem (Rahmaniani et al., 2017). We implement a BBC algorithm in which the MP is solved by a single search tree, and the cuts are generated within the tree. This strategy has yielded satisfactory results in different applications, including network design, transit systems, and transportation network recovery (see e.g., Gendron et al., 2016; Errico et al., 2017; Gouveia et al., 2018; Moreno et al., 2019, 2020).

Our proposed BBC embeds the resolution of the master problem and the subproblem in a branch-and-bound (B&B) tree, calling the subproblem when an integer solution is found as shown in Figure 3. At each node r of the branching tree, the linear relaxation of the current master problem (LP_r) is solved. The subproblem is then only solved if the corresponding solution is integer, feasible and has a better objective value (OF_r) than the objective value of the current incumbent (OF_r^*). Otherwise branching is performed if the solution is non-integer, while node r is pruned if the solution is infeasible or its corresponding objective value is higher than or equal to the objective value of the current incumbent. When the corresponding subproblem is solved, three possibilities can arise: 1) generating a violated feasibility Benders cut, 2) generating a violated optimality Benders cut, and 3) setting the LP_r solution as the new incumbent. A feasibility cut is violated and added to the MP if the subproblem is infeasible, whereas an optimality cut is violated and added to the MP if the subproblem is feasible and its objective function is higher than the objective function of the current MP (OF_r). If no cuts are generated, i.e., the subproblem is feasible and its objective function is equal to OF_r, LP_r is set as the new incumbent solution, with $\text{OF}_r^* = \text{OF}_r$, and the node is pruned. If a cut is generated, the described steps are applied again. Automatized cuts and heuristics available in general-purpose optimization software can be used at each node r as well, although they are not presented in Figure 3.

In the following, we first describe and model the Benders MP (Section 4.1.1). Then, we describe and model the Benders subproblem SP (Section 4.1.2) for the ENDPPTC. Finally, we formulate the optimality and feasibility cuts for the ENDPPTC (Section 4.1.3).

4.1.1 Master problem

In the ENDPPTC, the complicating variables are the binary variables corresponding to opening (or not) a shelter ($Z_i,\ i \in \mathcal{V}^{\mathsf{d}}$) as well as the number of lanes selected in each link ($L_{le},\ l \in \mathcal{L}_e, e \in \mathcal{E} \setminus \mathcal{E}^p$). Therefore, the Benders MP for the ENDPPTC consists of determining 1) the shelter location by considering the maximum number of shelters, 2) the number of lanes used on each link by considering the maximum number of lanes in contraflow.

To model the MP, the additional variable Θ is used and aims to compute the total evacuation time, which represents our objective function to be minimized. The MP can then be modeled as follows:

$$\text{(MP)} \quad \min \qquad \Theta, \tag{2a}$$

$$\text{s.t.} \quad (1m) - (1p), (1t), (1u),$$
$$\Theta \geq 0. \tag{2b}$$

Note that, initially, the lower bound for Θ is zero. Every time a solution is found for the MP, feasibility or optimality cuts are added, which will likely increase the lower bound of Θ.

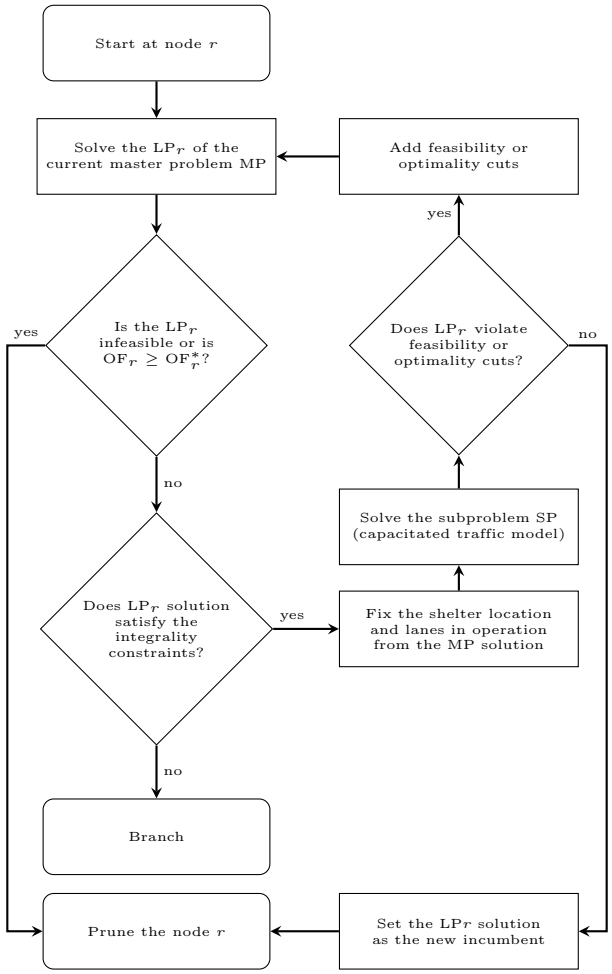

Figure 3: Flowchart illustrating the cut generation in a given node r of the branch-and-bound tree

4.1.2 Subproblem

Given the shelter location and routes defined in the MP, the subproblem entails determining the flow along the links across the time horizon, minimizing the total evacuation time. Thus, when the variables L_{le} and Z_i are fixed, the remaining problem becomes a LP model similar to the CTM proposed in the literature (Ziliaskopoulos, 2000; Zheng and Chiu, 2011), but with additional constraints related to the capacity of shelters and minimum flow on links. Let $\bar{Z}_i$ and $\bar{L}_{le}$ be the value of variables Z_i and L_{le} in the solution of the MP. The subproblem (SP) is defined as follows:

$$\text{(SP)} \quad \min \quad \sum_{j \in \mathcal{C} \setminus \{p\}} \sum_{t \in T^\tau} \tau X_{jt}. \tag{3a}$$

$$\text{s.t.} \quad (1b) - (1f), (1q) - (1s),$$
$$\sum_{k \in \Gamma_j} Y_{jkt} \leq \sum_{l \in \mathcal{L}_e} Q_{jlt} \bar{L}_{le}, \qquad \forall\, j \in \mathcal{C}_e, e \in \mathcal{E} \setminus \mathcal{E}^p, t \in T^\tau, \tag{3b}$$

$$\sum_{j\in\Gamma_k^{-1}} Y_{jkt} \le \sum_{l\in\mathcal{L}_e} Q_{klt}\bar{L}_{le}, \qquad \forall\, k\in\mathcal{C}_e, e\in\mathcal{E}\setminus\mathcal{E}^p, t\in T^\tau, \tag{3c}$$

$$\sum_{j\in\Gamma_k^{-1}} Y_{jkt} \le \sum_{l\in\mathcal{L}_e} \delta N_{klt}\bar{L}_{le} - \delta X_{kt}, \qquad \forall\, k\in\mathcal{C}_e, e\in\mathcal{E}\setminus\mathcal{E}^p, t\in T^\tau, \tag{3d}$$

$$\sum_{t\in T^\tau} Y_{jpt} \le K_i\bar{Z}_i, \qquad \forall\, j\in\mathcal{C}^{\mathtt{d}}, i\in\mathcal{V}^{\mathtt{d}} : n_{ji}=1, \tag{3e}$$

$$\sum_{t\in T^\tau}\sum_{k\in\Gamma_j^{-1}} Y_{kjt} \ge m^{\mathtt{e}}\sum_{l\in\mathcal{L}_e}\bar{L}_{le}, \qquad \forall\, j\in\mathcal{C}_e, e\in\mathcal{E}\setminus\mathcal{E}^p, \tag{3f}$$

$$\sum_{t\in T^\tau} Y_{jpt} \ge m^{\mathtt{d}}\bar{Z}_i, \qquad \forall\, j\in\mathcal{C}^{\mathtt{d}}, i\in\mathcal{V}^{\mathtt{d}} : n_{ji}=1. \tag{3g}$$

The objective function (3a) is written as for the ENDPPTC, i.e., (1a). Constraints (3b)–(3g) are similar to constraints (1g)–(1l), but variables L_{le} and Z_i are fixed according to the MP solution ($\bar{Z}_i$, $\bar{L}_{le}$).

4.1.3 Optimality and feasibility cuts

Every time an integer solution is found in the MP, the SP is solved. When the SP is solved, a dual solution is obtained. Let $\bar{\lambda}^{(1b)}_{ji}$, $\bar{\lambda}^{(3b)}_{jet}$, $\bar{\lambda}^{(3c)}_{jet}$, $\bar{\lambda}^{(3d)}_{jet}$, $\bar{\lambda}^{(3e)}_{ji}$, $\bar{\lambda}^{(3f)}_{je}$, and $\bar{\lambda}^{(3g)}_{ji}$ denote the values of the dual variables associated with constraints (1b), (3b), (3c), (3d), (3e), (3f), and (3g) upon solving the SP. Using these values, an optimality cut is generated if the suproblem is feasible and optimally solved, while a feasibility cut is generated if the subproblem is infeasible and dual unbounded. In the following, we formulate the optimality and the feasibility cuts.

Optimality cuts. If the subproblem is feasible and optimally solved, an extreme point is found. The following optimality cut is then added to the MP:

$$\begin{aligned}\Theta \ge\ & \sum_{j\in\mathcal{C}^{\mathtt{s}}}\sum_{\substack{i\in\mathcal{V}^{\mathtt{s}}:\\ n_{ji}=1}} b_i\bar{\lambda}^{(1b)}_{ji} + \sum_{j\in\mathcal{C}_e}\sum_{e\in\mathcal{E}\setminus\mathcal{E}^p}\sum_{t\in T^\tau}\sum_{l\in\mathcal{L}_e} Q_{jlt}L_{le}\bar{\lambda}^{(3b)}_{jet} + \sum_{j\in\mathcal{C}_e}\sum_{e\in\mathcal{E}\setminus\mathcal{E}^p}\sum_{t\in T^\tau}\sum_{l\in\mathcal{L}_e} Q_{jlt}L_{le}\bar{\lambda}^{(3c)}_{jet} \\ & + \sum_{j\in\mathcal{C}_e}\sum_{e\in\mathcal{E}\setminus\mathcal{E}^p}\sum_{t\in T^\tau}\sum_{l\in\mathcal{L}_e} \delta N_{jlt}L_{le}\bar{\lambda}^{(3d)}_{jet} + \sum_{j\in\mathcal{C}^{\mathtt{d}}}\sum_{\substack{i\in\mathcal{V}^{\mathtt{d}}:\\ n_{ji}=1}} K_iZ_i\bar{\lambda}^{(3e)}_{ji} \\ & - \sum_{j\in\mathcal{C}_e}\sum_{e\in\mathcal{E}\setminus\mathcal{E}^p}\sum_{l\in\mathcal{L}_e} m^{\mathtt{e}}L_{le}\bar{\lambda}^{(3f)}_{je} - \sum_{j\in\mathcal{C}^{\mathtt{d}}}\sum_{\substack{i\in\mathcal{V}^{\mathtt{d}}:\\ n_{ji}=1}} m^{\mathtt{d}}Z_i\bar{\lambda}^{(3g)}_{ji}.\end{aligned} \tag{4}$$

Feasibility cuts. If the subproblem is infeasible (i.e., dual unbounded), an extreme ray is found. The following feasibility cut is then added to the MP:

$$\begin{aligned}0 \ge\ & \sum_{j\in\mathcal{C}^{\mathtt{s}}}\sum_{\substack{i\in\mathcal{V}^{\mathtt{s}}:\\ n_{ji}=1}} b_i\bar{\lambda}^{(1b)}_{ji} + \sum_{j\in\mathcal{C}_e}\sum_{e\in\mathcal{E}\setminus\mathcal{E}^p}\sum_{t\in T^\tau}\sum_{l\in\mathcal{L}_e} Q_{jlt}L_{le}\bar{\lambda}^{(3b)}_{jet} + \sum_{j\in\mathcal{C}_e}\sum_{e\in\mathcal{E}\setminus\mathcal{E}^p}\sum_{t\in T^\tau}\sum_{l\in\mathcal{L}_e} Q_{jlt}L_{le}\bar{\lambda}^{(3c)}_{jet} \\ & + \sum_{j\in\mathcal{C}_e}\sum_{e\in\mathcal{E}\setminus\mathcal{E}^p}\sum_{t\in T^\tau}\sum_{l\in\mathcal{L}_e} \delta N_{jlt}L_{le}\bar{\lambda}^{(3d)}_{jet} + \sum_{j\in\mathcal{C}^{\mathtt{d}}}\sum_{\substack{i\in\mathcal{V}^{\mathtt{d}}:\\ n_{ji}=1}} K_iZ_i\bar{\lambda}^{(3e)}_{ji} \\ & - \sum_{j\in\mathcal{C}_e}\sum_{e\in\mathcal{E}\setminus\mathcal{E}^p}\sum_{l\in\mathcal{L}_e} m^{\mathtt{e}}L_{le}\bar{\lambda}^{(3f)}_{je} - \sum_{j\in\mathcal{C}^{\mathtt{d}}}\sum_{\substack{i\in\mathcal{V}^{\mathtt{d}}:\\ n_{ji}=1}} m^{\mathtt{d}}Z_i\bar{\lambda}^{(3g)}_{ji}.\end{aligned} \tag{5}$$

4.2 Enhancement strategies

In this section, two strategies to improve the performance of the BBC algorithm are presented. The first improvement strategy consists of formulating a stronger master problem (Section 4.2.1). The

second strategy consists of generating only a subset of variables and constraints in the subproblems according to the solution obtained from the improved master problem (Section 4.2.2). Note that the second strategy can only be used if the first strategy is used as it requires the solution of the stronger master problem.

4.2.1 Strengthened master problem MP*

In the original master problem, the information related to the flow decisions and the estimation of the traffic congestion is lost due to the decomposition. In this case, the subproblem can be called many times. Therefore, a large number of cuts can be generated which impacts the convergence of the algorithm. In general, the performance of the algorithm can be significantly affected by the quality of the initial bound obtained from the MP. For this reason, many strategies have been proposed to devise stronger master problem formulations and to retrieve part of the information lost in the decomposition (see e.g., Errico et al., 2017; Gendron et al., 2016; Moreno et al., 2020). In this section, we propose a stronger master problem formulation, referred to as MP*, by adding new variables and constraints to simulate the flow decisions and setting a lower bound for Θ.

The stronger master problem MP* is defined on the graph G over the set of time periods T^τ. It incorporates traffic-congestion parameters computed in the cell-representation graph G^τ. To properly define MP*, we introduce the sets $\mathcal{E}_i^-$ and $\mathcal{E}_i^+$, $\forall i \in \mathcal{V}$ which are defined as the set of incoming links to node $i \in \mathcal{V}$ (i.e., links starting at a node $\forall j \in \mathcal{V}, i \neq j$ and ending at i) and outgoing links from node $i \in \mathcal{V}$ (i.e., links starting at node i and ending at a node $\forall j \in \mathcal{V}, i \neq j$). For each period $t \in T^\tau$, we also define K_{elt} as the capacity of link $e \in \mathcal{E} \setminus \mathcal{E}^p$ given l lanes in operation, which is computed as $K_{elt} = \min\{\max_{i \in C_e}\{Q_{ilt}\}, \max_{i \in C_e}\{\delta N_{ilt}\}\}$. MP* can then be modelled using two additional sets of continuous variables, i.e., $\chi_{it}, i \in \mathcal{V}, t \in T$ and $v_{et}, e \in \mathcal{E}, t \in T^\tau$. For each period $t \in T^\tau$, we define χ_{it} as the number of vehicles at node $i \in \mathcal{V}$ at period t, and v_{et} as the number of vehicles travelling on link $e \in \mathcal{E}$ at period t. MP* can then be modelled as:

$$
\begin{aligned}
(\text{MP}^*) \quad \min \quad & \Theta, && && (6a)\\
\text{s.t.} \quad & (1\text{m}) - (1\text{p}), (1\text{t}), (1\text{u}) && && \\
& \Theta \geq \sum_{t \in T^\tau} \sum_{e \in \mathcal{E} \setminus \mathcal{E}^p} \tau \ell_e v_{et} + \sum_{t \in T^\tau} \sum_{i \in \mathcal{V} \setminus \{p\}} \tau \chi_{it} + \sum_{t \in T^\tau} \sum_{e \in \mathcal{E}_p^-} \tau v_{et}, && && (6b)\\
& \sum_{e \in \mathcal{E}_i^+} v_{e1} + \chi_{i1} = b_i, && \forall\, i \in \mathcal{V}^{\text{s}}, && (6c)\\
& \sum_{e \in \mathcal{E}_i^+} v_{et} + \chi_{it} = \sum_{\substack{e \in \mathcal{E}_i^- : \\ t - \ell_e > 0}} v_{e(t-\ell_e)} + \chi_{i(t-1)}, && \forall\, i \in \mathcal{V}^{\text{s}}, t \in T^\tau : t > 1, && (6d)\\
& \sum_{t \in T^\tau} \sum_{e \in \mathcal{E}_p^-} v_{et} = \sum_{i \in \mathcal{V}^{\text{s}}} b_i, && && (6e)\\
& \sum_{e \in \mathcal{E}_i^+} v_{et} + \chi_{it} = \sum_{\substack{e \in \mathcal{E}_i^- : \\ t - \ell_e > 0}} v_{e(t-\ell_e)} + \chi_{i(t-1)}, \; {\scriptstyle t>1} && \forall\, i \in \mathcal{V} \setminus \{\mathcal{V}^{\text{s}} \cup \{p\}\}, t \in T^\tau, && (6f)\\
& \sum_{t \in T^\tau} v_{et} \geq m^{\text{e}} \sum_{l \in \mathcal{L}_e} L_{le}, && \forall\, e \in \mathcal{E} \setminus \mathcal{E}^p, && (6g)\\
& \sum_{t \in T^\tau} v_{et} \geq m^{\text{d}} Z_i, && \forall\, e \in \{\mathcal{E}_i^+ \cup \mathcal{E}_p^-\}, i \in \mathcal{V}^{\text{d}}, && (6h)\\
& \sum_{t \in T^\tau} v_{et} \leq K_i Z_i, && \forall\, e \in \{\mathcal{E}_i^+ \cup \mathcal{E}_p^-\}, i \in \mathcal{V}^{\text{d}}, && (6i)\\
& v_{et} \leq \sum_{l \in \mathcal{L}_e} K_{elt} L_{le}, && \forall\, e \in \mathcal{E} \setminus \mathcal{E}^p, t \in T^\tau, && (6j)\\
& v_{et} \leq \delta \sum_{l \in \mathcal{L}_e} (\min_{j \in C_e}\{N_{jlt}\}) L_{le} - \delta v_{e(t-1)}, \; {\scriptstyle t>1} && \forall\, e \in \mathcal{E} \setminus \mathcal{E}^p, t \in T^\tau, && (6k)\\
& v_{et} \geq 0, && e \in \mathcal{E}, t \in T^\tau, && (6l)\\
& \chi_{it} \geq 0, && i \in \mathcal{V}, t \in T^\tau. && (6m)
\end{aligned}
$$

Constraints (6b) establish a lower bound for the total evacuation time, which is defined as the sum of the travel time on the links ($\sum_{t\in T^\tau}\sum_{e\in\mathcal{E}\setminus\mathcal{E}^p}\tau\ell_e\upsilon_{et}+\sum_{t\in T^\tau}\sum_{e\in\mathcal{E}_p^-}\tau\upsilon_{et}$) plus the waiting time on the nodes ($\sum_{t\in T^\tau}\sum_{i\in\mathcal{V}\setminus\{p\}}\tau\chi_{it}$). Constraints (6c) and (6d) set the flow of vehicles for each source node at periods $t=1$ and $t>1$, respectively. Note that travelling along a link $e\in\mathcal{E}$ requires a time ℓ_e. Constraints (6e) and (6f) set the flow of vehicles for the sink node and all other nodes, respectively. Constraints (6g) and (6h) establish the minimum flow on links and shelters to consider their operation. Constraints (6i) ensure that the number of vehicles evacuated to each shelter respects its capacity. Constraints (6j) and (6k) state that the flow on a link $e\in\mathcal{E}\setminus\mathcal{E}^p$ is bounded by its capacity, according to the number of lanes in operation. Finally, constraints (6l) and (6m) define the domain of the decision variables. Note that MP* has a stronger lower bound than MP, but is more difficult to solve, particularly when considering small values of τ.

4.2.2 Improved subproblem SP*

The subproblem SP becomes computationally intractable when considering small time steps (τ), as smaller time steps result in more cells and time periods. In this section, we propose a strategy to reduce the complexity of the subproblems using the information when solving MP*. We refer to this subproblem as SP*. This strategy can only be used if we solve MP*.

When solving MP*, we obtain a solution with flows on the links. Using the optimal solution found when solving MP*, we reduce the cell-representation graph G^τ on which SP and SP$_h$ are solved by generating cells representing links on which there is a strictly positive flow of evacuees in the solution. Let $\bar{\chi}_{it}$ and $\bar{\upsilon}_{et}$ be the value of variables χ_{it} and υ_{et} in the optimal solution of the MP*. In the subproblems, we then generate only the variables $X_{jt}, j\in\mathcal{C}_e, t\in T^\tau$ such that $\sum_{t'\in T^\tau}\bar{\upsilon}_{et'}>0$ and the variables $Y_{kjt}, j\in\mathcal{C}_e, k\in C_{e'}, k\neq j, t\in T^\tau$ such that $\sum_{t'\in T^\tau}\bar{\upsilon}_{et'}>0$ and $\sum_{t'\in T^\tau}\bar{\upsilon}_{e't'}>0$. This strategy allows to reduce the size of the subproblem. In addition, we still guarantee that optimal solutions can be found for the subproblem because we eliminate cells that would not be used anyway.

5 Computational results

This section describes the instance generation methodology (Section 5.1), analyzes how different time step values affect the traffic impact estimation (Section 5.2), compares the computational performance of the proposed formulation and solution methods (Section 5.3), assesses the impact of how traffic is modeled in the evacuation time (Section 5.4), and analyzes the solutions in light of different parameter variations (Section 5.5). In this section, we report summarized results. Detailed results can be accessed at Mendeley data (Moreno et al., 2023). All the algorithms were coded in C++ and run on a PC with an Intel Gold 6148 Skylake processor with 16.0 GB of RAM and a single thread. The MIP and LP models were solved using IBM CPLEX Optimization Solver 20.1. Benders cuts are added using the Callback classes available in the Concert Technology Library. We impose a computational time limit of 10,800 seconds, and the stopping criterion was either the elapsed time exceeding the time limit or the optimality gap being smaller than 10^{-4}. All the remaining parameters of CPLEX were kept at their default values.

5.1 Instance description

In this section, we describe the instances. We start by detailing how we have generated the different networks inspired by real network configurations. Then, we specify the different parameters. The instance data files are publicly available at Mendelay data (Moreno et al., 2023), and the algorithm for generating instances is available upon request.

5.1.1 Network structure

The instances were randomly generated based on procedures previously used in the literature and inspired by real network configurations (Masucci et al., 2009; Zheng and Chiu, 2011; Ulusan and

Ergun, 2018; He et al., 2018; Esposito Amideo et al., 2021). A total of 144 networks are generated, with different topologies, areas, and source and destination nodes location. In the following, we first describe the four network topologies. Then, we explain how the nodes including the source nodes ($\mathcal{V}^{\mathrm{s}}$), the destination nodes ($\mathcal{V}^{\mathrm{d}}$) and the intersection nodes ($\mathcal{V}^{\mathrm{u}}$) have been generated. Finally, we detail the generation of the directed links representing the roads ($\mathcal{E} \setminus \mathcal{E}^p$).

The instances are divided into four classes based on their topology: Grid (G), Grid-like (L), Irregular (I), and Sparse (S). These topologies simulate real-road networks. For example, Boston and Manhanttan road networks can be represented using irregular and grid-like network topologies (Ulusan and Ergun, 2018), respectively, whereas remote villages can be represented using sparse networks. For each topology, nine different rectangular areas, referred to as sizes, $(h \times w)$ are generated, where h represents the height and w represents the width of the area. The generated areas are $(3 \times 12), (4 \times 9), (4 \times 15), (5 \times 12), (6 \times 6), (6 \times 10), (6 \times 20), (8 \times 15), (10 \times 12)$. The instances are referred to as X $(h \times w)$, where X represents the topology and $(h \times w)$ indicates the size of the area. For example, G (3×12) refers to a Grid topology on a (3×12) rectangular area. Figure 4 illustrates an example of these four topologies on a rectangular area of (8×15).

G, L, and I networks have $h \times w$ nodes, while S networks have $\lceil 0.4 \cdot h \times w \rceil$. The nodes in the G and L topologies are positioned equidistantly in the rectangular area, while in the I and S topologies they are randomly positioned (see Figure 4). Each generated node is either a source node ($\mathcal{V}^{\mathrm{s}}$), a destination node ($\mathcal{V}^{\mathrm{d}}$), or an intersection node ($\mathcal{V}^{\mathrm{u}}$), and $\mathcal{V}^{\mathrm{s}} \cup \mathcal{V}^{\mathrm{d}} \cup \mathcal{V}^{\mathrm{u}} = \emptyset$. The number of generated source and destination nodes depends on the area size. Specifically, the number of destination nodes is given by $|\mathcal{V}^{\mathrm{d}}| = \lfloor 0.1 \cdot (h \times w) \rfloor$, while the number of source nodes is given by $|\mathcal{V}^{\mathrm{s}}| = \lfloor 0.07 \cdot (h \times w) \rfloor$. The nodes $\mathcal{V}^{\mathrm{s}}$ and $\mathcal{V}^{\mathrm{d}}$ are randomly located in area considering two configurations: *aside* and *surrounding*. In *aside* configuration, the source and destination nodes are located at the opposite sides of the rectangular area. These configurations represent disasters, such as Tsunamis in near-coastal ocean regions, where people need to be evacuated to the opposite side of the city. In *surrounding* configurations, source nodes are located in the center of the area, while destination nodes are located on the outskirts of the area. Surrounding configurations represent, for example, flood evacuations where people in low-lying areas need to be evacuated to high-lying areas. For both configurations, there are no destination nodes located within a radius r (measured in miles) of a source node, and two values of $r = \{3, 5\}$ are tested. Figure 5 illustrates these two configurations on a sparse topology.

In the G, L, and I topologies, the number of roads is $(h-1) \cdot w + (w-1) \cdot h$ (i.e., $|\mathcal{E} \setminus \mathcal{E}^p| = 2 \cdot [(w-1) \cdot h + (h-1) \cdot w]$), while the S topologies have $\lceil 0.4 \cdot [(w-1) \cdot h + (h-1) \cdot w] \rceil$ roads (i.e., $|\mathcal{E} \setminus \mathcal{E}^p| = 2 \cdot \lceil 0.4 \cdot [(w-1) \cdot h + (h-1) \cdot w] \rceil$). In addition, the length μ_e of each link $e \in \mathcal{E} \setminus \mathcal{E}^p$ is one unit of distance $\mu_e = 1$ in the G topology, while it can go up to two units of distance ($\mu_e \leq 2$) in the L, I and S topologies. The arcs are generated using the generation procedure to build Erdös-Rényi Planar Graphs (Masucci et al., 2009). The roads are classified into three categories: freeways, arterial streets and local streets (similar to He et al., 2018). Freeways and arterial streets traverse the networks from left to right and from bottom to top. The number of freeways and arterial streets is calculated based on the width and height of the rectangular area, as well as the network topology. Specifically, in the G, L, and I topologies, the number of freeways from left to right is $\lfloor h/7 \rfloor$, and from bottom to top is $\lfloor w/7 \rfloor$. In contrast, in the S topology, these numbers are $\max 0, \lfloor h/7 \rfloor - 1$ and $\max 0, \lfloor w/7 \rfloor - 1$, respectively. In addition, in the G, L, and I topologies, the number of arterial streets from left to right are $\lfloor h/4 \rfloor$, and from bottom to top are $\lfloor w/4 \rfloor$, while these numbers are $\min\{0, \lfloor h/4 \rfloor - 1\}$ and $\min\{0, \lfloor w/4 \rfloor - 1\}$ in the S topology. In addition, we ensure that freeways and arterial streets have a continuous path (see Appendix B for more details). Figure 6 illustrates a L(8×15) instance with its specific freeways, arterial streets and local streets.

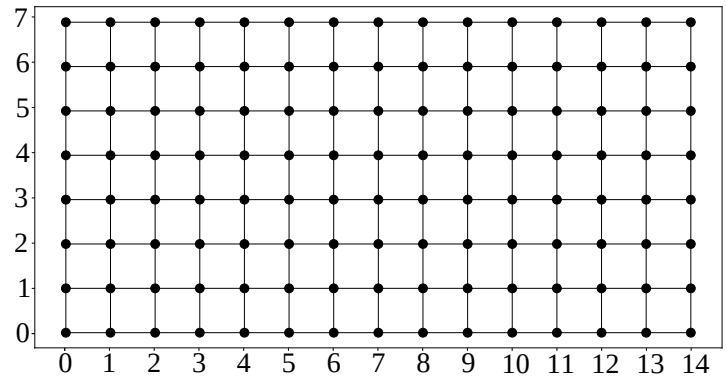

(a) Grid topology (G)

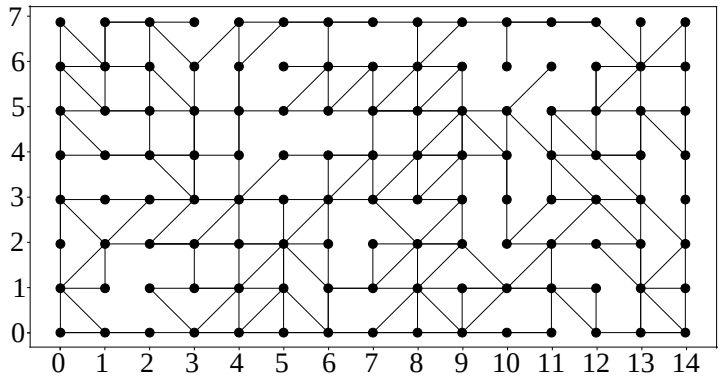

(b) Grid-like topology (L)

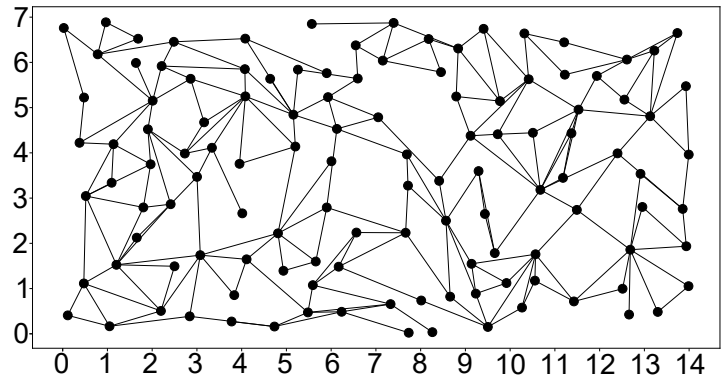

(c) Irregular topology (I)

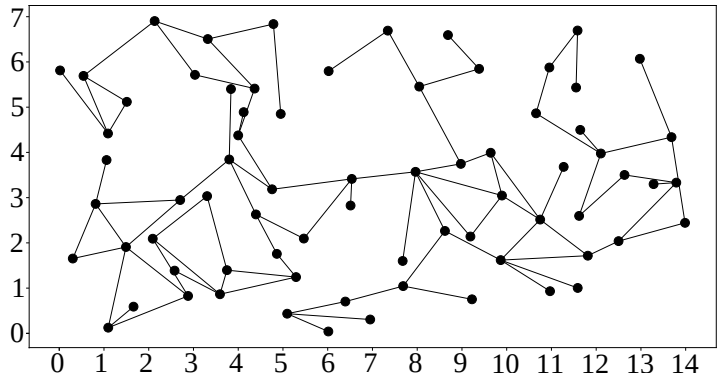

(d) Sparse topology (S)

Figure 4: Example of four instances G(8×15), L(8×15), I(8×15), and S(8×15)

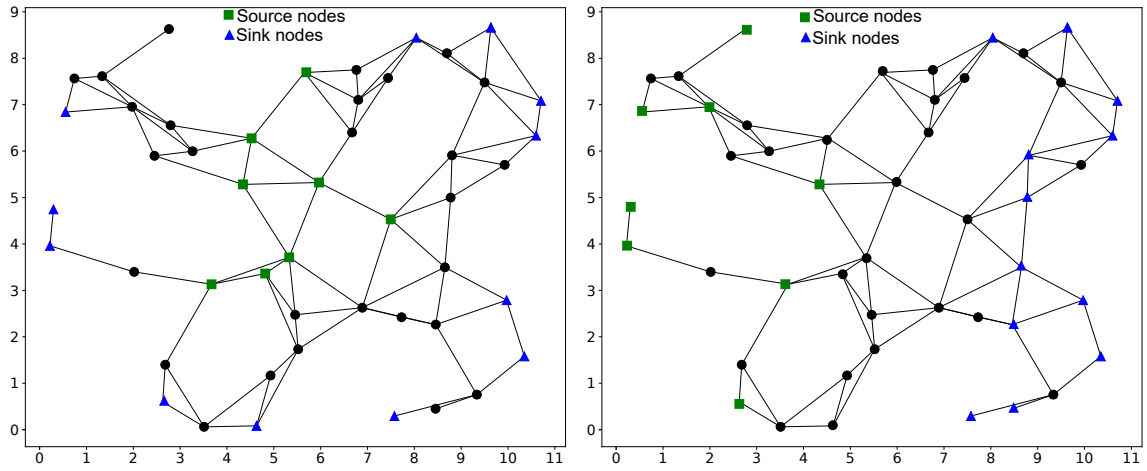

(a) Surrounding configuration (b) Aside configuration

Figure 5: Example of a aside and surrounding configurations with instance S(10×12)

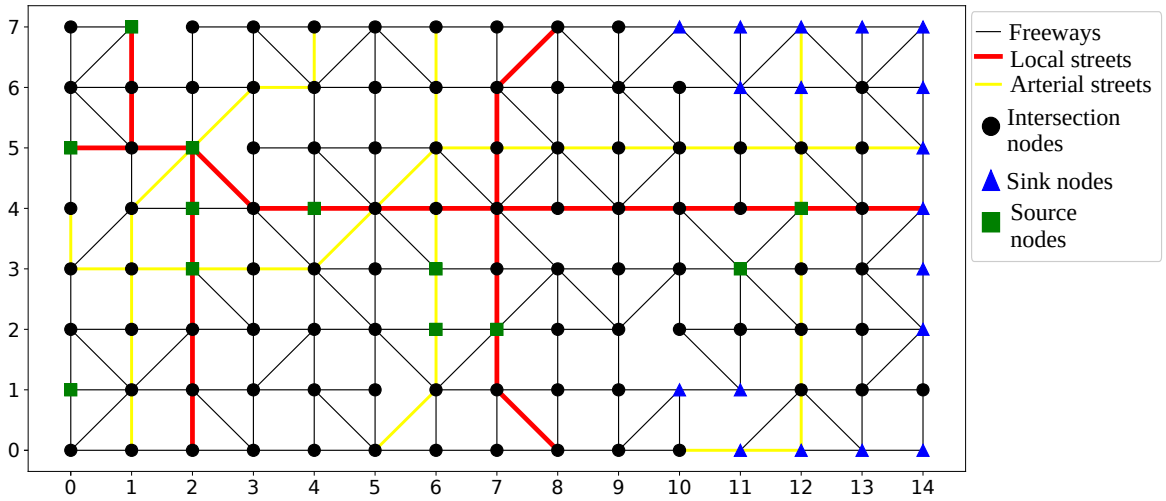

Figure 6: Example of freeways, arterial streets and local streets, L(8×15)

5.1.2 Parameters

In this section, we specify the different parameters that have been used in our experiments. We first specify the parameters related to the nodes as well the maximum number of shelters. Then, we describe the parameters related to the links. Finally, we define the traffic congestion parameters. Note that in the traffic congestion parameters, we do not discuss the value of the time step (τ) as different values have been tested to assess the quality of the solutions and the performance of the algorithm (see Section 5.2).

Each source node $i \in \mathcal{V}^{\mathtt{s}}$ has a demand b_i representing the number of vehicles to be evacuated. The values of b_i were generated following the method used by Esposito Amideo et al. (2021), specifically from an integer uniform distribution between 50 and 550 vehicles, i.e., $b_i \sim \mathcal{U}(50, 550), \forall i \in \mathcal{V}^{\mathtt{s}}$. In addition, destination node has a capacity $(K_i, i \in \mathcal{V}^{\mathtt{d}})$ computed as

$$K_i = \frac{\sum_{k \in \mathcal{V}^{\mathtt{s}}} b_k}{\phi \cdot \mathtt{K}}, \forall i \in \mathcal{V}^{\mathtt{d}},$$

where ϕ is a weighting parameter set to 0.8 as in Esposito Amideo et al. (2021). In addition, the minimum number of vehicles that can be sent during the evacuation to a destination node is set to 5% of the total demand, that is, $m^{\mathtt{d}} = 0.05 \sum_{i \in \mathcal{V}^{\mathtt{s}}} b_i$. The maximum number of shelters is set as $\mathtt{K} = |\mathcal{V}^{\mathtt{d}}|$.

Each generated road is represented by two directed links in $\mathcal{E} \setminus \mathcal{E}^p$. As detailed in Section 5.1.1, each road has a category: freeway, arterial street and local street. According to its category, its links have different values: i) the free-flow capacity (q_e), ii) the free-flow speed (v_e), and iii) the number of available lanes (f_e). Table 2 defines the values q_e, v_e, and f_e according to its category. In addition, the maximum number of lanes that can be used for contraflow operations in link $e \in \mathcal{E} \setminus \mathcal{E}^p$ is computed as $f_e^{\mathtt{M}} = f_e - 1$, and the maximum number of links in contraflow is computed as $E = |\mathcal{E} \setminus \mathcal{E}^p|/2$. Finally, if a link is selected for the evacuation, the minimum number of vehicles that can be sent over that link during the evacuation is set to 1% of the total demand, that is, $m^{\mathtt{e}} = 0.01 \sum_{i \in \mathcal{V}^{\mathtt{s}}} b_i, \forall e \in \mathcal{E} \setminus \mathcal{E}^p$.

Table 2: Parameters for each link category

Link category	Capacity (q_e)	Free-flow speed (v_e)	# lanes (f_e)
Freeway	1800 veh/h/lane	65 mph	3
Arterial street	1200 veh/h/lane	40 mph	2
Local street	600 veh/h/lane	30 mph	1

For the traffic congestion parameters, the value of the traffic jam density is set to 180 vehicles per mile per lane ($\kappa = 180$). In addition, for each cell $i \in \mathcal{C}_e, e \in \mathcal{E} \setminus \mathcal{E}^p$, the ratio between the backward wave speed and free-flow speed is set to 0.3 ($\delta = 0.3$). These values are averages based on the literature (Li et al., 2003; Ziliaskopoulos, 2000; Zheng and Chiu, 2011). Finally, we have set the time horizon T^τ to allow for the evacuation of the total demand. At period $t = 0$, we set the initial state of the system with 0 vehicles in each cell ($X_{j0} = 0, \forall j \in \mathcal{C}$) and with 0 vehicles moving from a cell to another cell ($Y_{jk0} = 0, \forall j \in \mathcal{C}, k \in \Gamma_j$). In the G, L, and I networks, the time horizon is set to 1.5 hours, while it is set to 2 hours in the S networks.

5.2 Analysis of time step τ

In this section, we tested different values for the time step τ, ranging from 6 to 30 based on the literature (He et al., 2018; Mohebifard and Hajbabaie, 2019; Zheng and Chiu, 2011). Figure 7 reports the average computational time (in seconds) as well as the percentage of feasible and optimal solutions obtained with our solution approach for different values of τ. Note that for instances that are not solved to optimality within the 10,800-second time limit, we use 10,800 seconds to compute the average computational time. Figure 8 reports the impact on the solution quality (i.e., the value of the total evacuation time) for different values of τ. More precisely, this is computed as $(z_\tau - z_6)/z_6$ where z_τ and z_6 are the values of the total evacuation time with the tested values of τ, i.e., $\{6, 9, 12, 15, 18, 21, 24, 27, 30\}$, and when setting $\tau = 6$. We report the average over all the instances that are solved to optimality for all the tested values of τ.

On the one hand, the results show that when increasing the value of τ, this decreases the complexity of the algorithm, i.e., more instances are solved within shorter computational time. As a general trend, for every increment of 3 of τ between 6 and 18, 12% and 14% additional instances are solved to feasibility and optimality, with an average computational time decrease of 1,659 seconds. For every increment of 3 of τ between 18 and 30, the number of instances solved (feasible and optimal solutions) remain stable, with an average computational time decrease of 191 seconds. Our solution approach can solve only 44% of instances to optimality with $\tau = 6$, whereas more than 98% of instances are solved to optimality with $\tau \geq 18$, and 100% of instances are solved to optimality with $\tau = 30$. In addition, the average computational time decreases from 7,748 seconds with $\tau = 6$ to 348 seconds with $\tau = 30$.

On the other hand, the results show that when increasing the value of τ, this reduces the quality of the solution, i.e., the evacuation time is overestimated. When going from $\tau = 6$ to $\tau = 30$, the total evacuation time is overestimated by 8.0%, 5.4%, 9.4%, 4.8% for the G, L, I, and S networks. Note

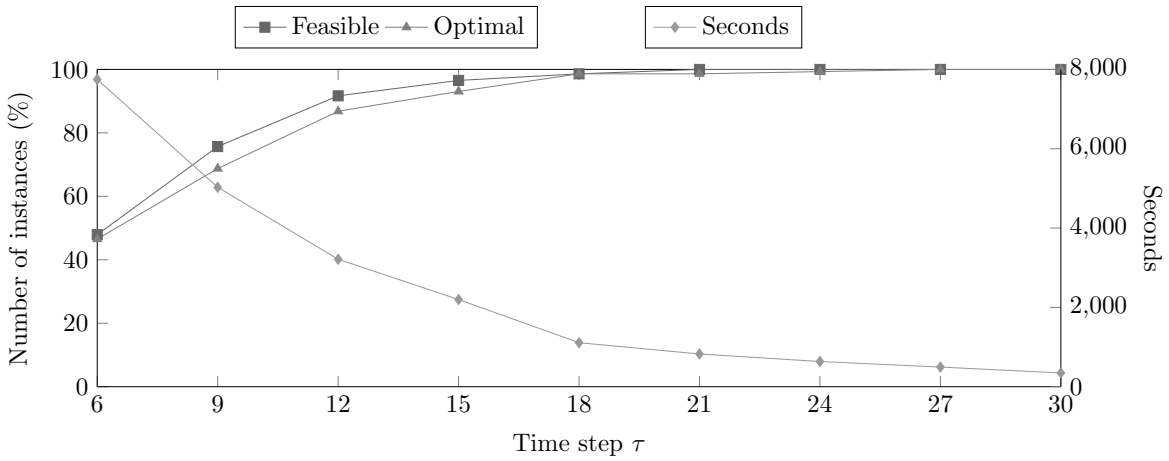

Figure 7: Average run time and percentage of feasible and optimal solutions obtained by our BBC for different time steps

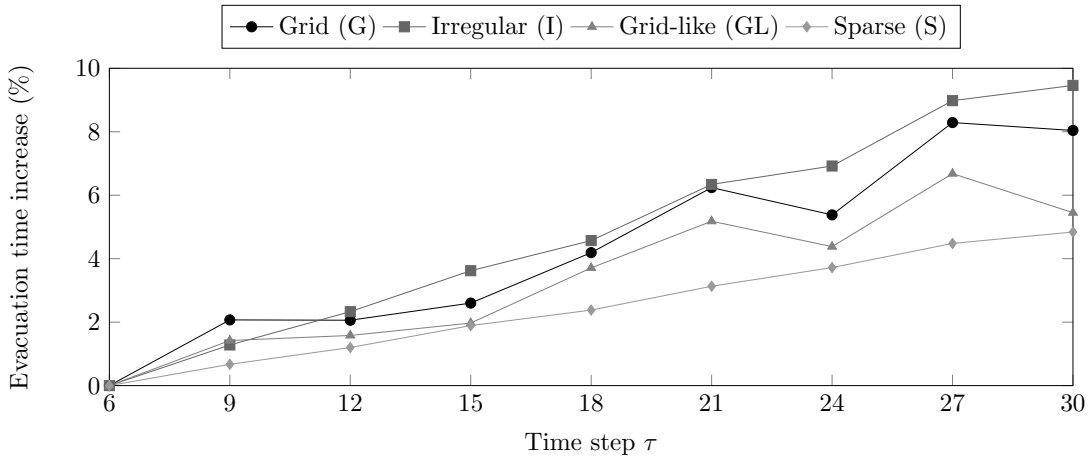

Figure 8: Impact of τ on the estimation of the total evacuation time (objective function)

that for the G and L networks, increasing the value of τ sometimes yields a reduction of the total evacuation time, e.g., when going from $\tau = 21$ to $\tau = 24$ the total evacuation time is overestimated by an average of 6.2% and 5.4% for G networks, and 5.2% and 4.4% for L networks. This is due to the fact that a larger time step (τ) increases the link capacities (Q_{ilt}, N_{ilt}). As a general trend, this overestimation is the lowest for sparse (S) networks and the highest for irregular (I) networks. Considering both solution quality and algorithmic complexity, setting $\tau = 18$ provides a reasonable trade-off, yielding a sufficiently accurate solution within a reasonable time frame. In fact, when fixing $\tau = 18$, 98.6% of the instances are solved to optimality with an average computational time of 1,110 seconds. In addition, compared with $\tau = 6$, the overestimation of the evacuation time is less than 5% on average. Therefore, in the following sections, we fix $\tau = 18$.

5.3 Computational performance of our BBC

In this section, we first compare our complete BBC (with the two enhancement strategies) with three other solution algorithms: i) a MIP, ii) the BBC without reducing the complexity of the subproblem, and iii) the BBC with no improvement strategies. Second, using our complete BBC, we analyze its performance on the different network sizes and topologies. Note that the average computational time is computed by considering a time of 10,800 seconds for instances that are not solved to proven optimality within the time limit.

5.3.1 Comparison between our BBC and other solution algorithms

In this section, we analyze the performance of our Benders decomposition algorithm, referred to as *our BBC*. Our BBC includes all enhancement strategies proposed in Section 4.2, including solving the stronger master problem MP*, as introduced in Section 4.2.1, and reducing the complexity of the subproblem, i.e., SP* as introduced in Section 4.2.2. First, we compare it with solving Model (1) (using IBM CPLEX Optimization Solver 20.1), referred to as *MIP*. Second, we analyze the impact of considering the two proposed enhancement strategies. More precisely, we solve two variants of the BBC: 1) a variant where no improvement strategies are used, referred to as *Basic BBC*, that is with MP and SP, and 2) a variant where the stronger master problem is solved without reducing the complexity of the subproblem, referred to as *BBC with MP**, that is with MP* and SP. Note that as explained in Section 4.2.2, to reduce the complexity of the subproblem, it is necessary to solve MP*. Therefore, we cannot test a variant where we reduce the complexity of the subproblem and solve the basic master problem MP.

Table 3 reports the following information: the percentage of instances for which a feasible solution is found (*%Feas*); the percentage of instances which are solved to proven optimality (*%Opt*); the average computational time in seconds (*Sec.*); the percentage of the computational time spent in the branch-and-bound tree (*% Time B&B*); the percentage of the computational time spent to solve the subproblem (*% Time SP*); the average number of nodes explored in the branching tree (# B&B nodes); and the average number of subproblems that are solved (# SP solved). Also, we compute % Time B&B, % Time SP, # B&B nodes, and # SP solved over optimal solutions.

Table 3: Average results of the proposed exact methods over 144 instances with $\tau = 18$

Method	%Feas	%Opt	Sec.	% Time B&B	% Time SP	# B&B nodes	# SP solved
MIP	36.8	35.4	8,274	–	–	0.5	–
Basic BBC (MP-SP)	0.0	0.0	10,800	–	–	–	–
BBC with MP* (MP*-SP)	94.4	94.4	1,347	41.7	58.3	24.5	1.5
Our BBC (MP*-SP*)	100.0	98.6	1,110	47.6	52.4	36.3	1.6

Our results show that our BBC outperforms all other tested methods. In particular, it solves all instances to feasibility. It also solves the most instances to optimality (98.6%) and is the fastest (1,110 seconds on average). When removing the improvement strategy for the subproblem, i.e., BBC with MP*, the total computational time increases by an average of 237 seconds and 4.2% of the instances which were solved to optimality with our BBC cannot be solved to optimality. When removing both improvement strategies (Basic BBC), this is the worse solution algorithm as no instances can be solved to feasibility and optimality. With the basic BBC, there is no information about the flow decisions in the master problem, and solving the subproblem often yields an infeasible solution. Finally, while the MIP outperforms the basic BBC, it performs worse than BBC with MP* and our BBC. The performance of the MIP can be explained due to large number of cells and periods required to incorporate traffic congestion in the model. For many instances, the MIP is unable to solve the linear relaxation within the 10,800-second time limit. More precisely, only 36.8% and 35.4% of the instances can be solved to feasibility and optimality, compared with 94.4% and 94.4% for BBC with MP*, and with 100.0% and 98.6% for our BBC. In addition, the average computational time increases to 8,274 seconds (compared with 1,347 seconds for BBC with MP* and 1,110 for our BBC).

In addition, when analyzing the results obtained with BBC with MP* and our BBC, we see that the number of subproblems is small (1.6 on average for both algorithms) compared with the number of branching nodes (on average between 24.5 and 36.3). This can be explained by the fact that to solve the subproblem, the master problem needs to yield an integer solution. In our branching tree, solving the master problem often yields a non-integer solution, and therefore branching is performed. In addition, solving the subproblem is the most time-consuming part of our BBC, i.e., on average 1.6 subproblems are solved and require 52.5% of the total computational time.

Our results highlight the need to develop a sophisticated solution algorithm, and in particular the need to strengthen the formulation of the master problem for the BBC. Having a stronger master problem by retrieving information that was lost in the decomposition, significantly improves the performance of the BBC algorithm. In addition, solving the subproblem, i.e., estimating the traffic, is the most time-consuming part. Therefore, it is also important to find methods to reduce the complexity of the subproblem and to limit the number of times it is solved.

5.3.2 Impact of the network size and topology on the algorithmic performance

In this section, we analyze the performance of our BBC (with MP* and SP*) according to the size and the topology of the network. Tables 4 and 5 report the computational results of our BBC for different network topologies and sizes, respectively. In both tables we report: the percentage of instances which are solved to proven optimality (*%Opt*); the average computational time in seconds (*Sec.*); the percentage of the computational time spent in the branch-and-bound tree (*% Time B&B*); the percentage of the computational time spent to solve the subproblem (*% Time SP*); the average number of nodes explored in the branching tree (# B&B nodes); and the average number of subproblems that are solved (# SP solved). Note that we do not report the percentage of instances for which a feasible solution is found as it is 100.0%.

Table 4: Average results of our BBC for different network topologies

Topology	%Opt	Sec.	% Time B&B	% Time SP	# B&B nodes	# SP solved
Grid (G)	100.0	1,377	58.5	41.5	60.9	2.3
Irregular (I)	100.0	621	46.8	53.2	19.0	1.3
Grid-like (L)	100.0	1,230	54.1	45.9	52.4	1.6
Sparse (S)	94.4	1,211	30.9	69.1	10.7	1.3

Table 5: Average results of our BBC for different network sizes

	Size	%Opt	Sec.	% Time B&B	% Time SP	# B&B nodes	# SP solved
$h \times w = 120$	6×20	93.8	3,660	43.3	56.7	53.5	1.7
	8×15	93.8	2,809	47.5	52.5	124.2	2.3
	10×12	100.0	2,002	59.8	40.2	62.4	2.9
$h \times w = 60$	4×15	100.0	631	28.8	71.2	8.1	1.6
	5×12	100.0	320	44.9	55.1	14.3	1.6
	6×10	100.0	361	57.2	42.8	49.6	1.3
$h \times w = 36$	3×12	100.0	106	66.5	33.5	6.0	1.1
	4×9	100.0	56	31.8	68.2	1.0	1.1
	6×6	100.0	44	53.9	46.1	2.7	1.0

First, our results show that S networks are the hardest to solve, with 94.4% of instances with proved optimality, which can be explained by the fact that they have a longer time horizon, while I networks seem to be the easiest to solve. In addition, for the G and L networks, our BBC spends more time solving the B&B tree, while for the I and S networks solving the subproblems requires more time. Particularly, solving the subproblems in S networks requires twice as much time as solving the B&B tree.

Second, increasing the size of the network increases the complexity of the problem. In networks with $h \times w = 120$, the average run time is 2,824 seconds, while in networks with $h \times w = 60$ and $h \times w = 36$, the average run times are 437 and 69 seconds, respectively. Furthermore, the complexity of the problem also depends on the value of h/w, i.e., as h/w increases the computational time decreases. As an example, for instances with $h \times w = 120$, the average computational time is 3,660

seconds with 6×20 ($h/w = 0.3$), 2,809 seconds with 8×15 ($h/w = 0.53$) and 2,002 seconds with 10×12 ($h/w = 0.83$). In fact, as the value of h/w increases, the source and destination nodes are usually closer which reduces the complexity of the problem.

5.4 Impact of traffic congestion

In the ENDPPTC as modeled with (1a)–(1u), the location of shelters (modeled with Z_i) and the lanes used during the evacuation (modeled with L_{le}) are determined by considering traffic congestion in the network using a CTM approach. In this section, we refer to this problem as the ENDPPTC-CTM and aim to compare the results obtained with a better traffic estimation (using the CTM approach) with more standard approaches that have been developed in the literature. We first solve the evacuation network design planning problem without traffic congestion (ENDPP) using a mono-period flow location-allocation problem where the travel time is not affected by traffic (i.e., no traffic is incurred and therefore there is no waiting time) and the objective consists of minimizing the total evacuation time as

$$\min \sum_{e \in \mathcal{E}} \tau \ell_e X_e,$$

where X_e if the flow of vehicles on link $e \in \mathcal{E}$. We also model the ENDPPTC with a mono-period flow location-allocation problem where traffic is estimated using the Bureau of Public Roads (BPR) function (Afkham et al., 2022; Bayram and Yaman, 2018b), and refer to this as the ENDPPTC-BPR. The BPR function is commonly used in transportation planning and traffic engineering to model travel time on a road segment as a function of the road's capacity and traffic volume. The function accounts for the increase in travel time due to congestion. The objective can then be modeled as

$$\min \sum_{e \in \mathcal{E}} \tau \ell_e X_e \left(1 + \alpha \left(\frac{X_e}{U_e}\right)^{\beta}\right),$$

where U_e is the practical capacity of the link $e \in \mathcal{E}$ (maximum flow rate, in vehicles per hour), and $\alpha \geq 0, \beta \geq 0$ are parameters defined in accordance with the road characteristics (Bayram and Yaman, 2018a), and they are taken as $\alpha = 0.15$ and $\beta = 4$ as in previous works in the literature (Bayram and Yaman, 2018a,b; Kongsomsaksakul et al., 2005; Sherali et al., 1991). This objective function is non-linear, but we linearize it using a piecewise linear approximation as in Afkham et al. (2022). Appendix C provides the detailed models for the ENDPP and the ENDPPTC-BPR.

For the ENDPP and the ENDPPTC-BPR, Table 6 report for each network topology and size the following information: i) the percentage of evacuation time underestimation (Δ *Evac. time %*) which is computed for each instance as $(z^* - z')/z^*$, where z^* is the optimal solution value found when solving the ENDPPTC-CTM and z' is the optimal solution value found when solving the ENDPP or the ENDPPTC-BPR, respectively, and reported as an average over all instances; ii) the percentage of the CTM-based evacuation time overestimation (Δ *CTM time %*) which is computed for each instance as $(z'' - z^*)/z^*$, where z'' is the optimal solution value found when solving the ENDPPTC-CTM by fixing the shelter location ($Z_i, i \in \mathcal{V}^{\mathrm{d}}$) and the lanes used during the evacuation ($L_{el}, e \in \mathcal{E} \setminus \mathcal{E}^p, l \in \mathcal{L}_e$) with the optimal solution values ($\bar{Z}_i, i \in \mathcal{V}^{\mathrm{d}}$ and $\bar{L}_{el}, e \in \mathcal{E} \setminus \mathcal{E}^p, l \in \mathcal{L}_e$) found when solving the ENDPP or the ENDPPTC-BPR, respectively, and reported as an average over all instances.

Our results show that, on average, when ignoring the traffic in the evacuation time, i.e., ENDPP, or estimating it using a BPR function ENDPPTC-BPR, the evacuation time is underestimated by 42.1% and by 40.8%. Similarly, when fixing the shelter locations and the lanes used during the evacuation for the ENDPPTC-CTM with the values found when solving the ENDPP and the ENDPPTC-BPR, this increases the evacuation time by an average of 41.3% and by 26.3%. In addition, the impact on the sparse (S) networks is the most important, which can be explained by the fact that these networks have fewer roads and, consequently, fewer options to deviate traffic. For these, the total evacuation time was underestimated by more than 53% on average, and fixing the values of the shelter locations and the lanes used during the evacuation yielded an increase of more than 17% on average. Finally,

Table 6: Impact on the evacuation time estimation when comparing the ENDPPTC-CTM with the ENDPP and ENDPPTC-BPR

		ENDPP		ENDPPTC-BPR	
		Δ Evac. time (%)	Δ CTM time (%)	Δ Evac. time (%)	Δ CTM time (%)
Topology					
Grid (G)		35.6	45.2	35.0	29.7
Irregular (I)		37.2	45.5	36.1	30.0
Grid-like (L)		39.4	35.9	38.6	27.8
Sparse (S)		56.2	38.5	53.5	17.7
Size					
$h \times w = 120$	6×20	38.4	48.1	36.5	26.6
	8×15	36.1	53.5	34.4	30.0
	10×12	35.8	40.3	35.0	27.2
$h \times w = 60$	4×15	48.4	49.4	45.9	21.9
	5×12	41.8	42.2	40.8	24.3
	6×10	43.0	37.9	41.8	26.7
$h \times w = 36$	3×12	42.1	32.8	41.4	27.6
	4×9	46.2	31.4	44.9	26.8
	6×6	47.4	35.8	46.4	25.8
Average		42.1	41.3	40.8	26.3

with larger networks, i.e., networks with larger values of $h \times w$, the underestimation of the evacuation time is less important than for smaller networks. For the ENDPP and the ENDPPTC-BPR, the real evacuation time increases by at most 38.4% and 36.5% for the larger networks ($h \times w = 120$), while it increases by at most 48.4% and 46.4% for the smaller networks ($h \times w = 60$ and $h \times w = 36$). This can be explained by the fact that smaller networks have a smaller number of roads which limits the potential evacuation paths.

Our results suggest that properly estimating traffic during an evacuation is important as the resulting solutions are greatly affected by this estimation. Properly estimating traffic is also important in sparse networks like in rural areas where traffic can also become an issue due to the restricted road network. In fact, while the BPR function allows to capture partly the traffic incurred during the evacuation, the results obtained are close to not considering traffic. Nonetheless, solving the ENDPPTC-CTM is more difficult than solving the ENDPP and EPPTC-BPR: the computational time to solve ENDPPTC-CTM is on average 16 times the computational time required to solve the ENDPP and ENDPPTC-BPR. While the CTM approach is more complex, it allows to better represent traffic congestion and to provide better evacuation time estimates.

5.5 Solution analyses

In this section, we analyze the solutions according to different performance indicators which are defined as follows: i) the total evacuation time in hours (*Evac. time*), i.e., objective function (1a); ii) the total travel time and waiting time as a percentage of the total evacuation time (*% Travel* and *% Waiting*); iii) the maximum evacuation duration in hours (*Max evac. duration*), which represents the maximal

time required to evacuate the demand and is be computed as

$$\tau/3600 \cdot \min\left\{t \in T^{\tau} : \bar{X}_{pt} = \sum_{i \in \mathcal{V}^{\mathtt{s}}} b_i\right\},$$

where $\bar{X}_{pt}$ is the value of variable X_{pt} in the solution of the ENDPPTC; and iv) the percentage of opened shelters (*% Shelters used*), which is computed as

$$\frac{\sum_{i \in \mathcal{V}^{\mathtt{d}}} \bar{Z}_i}{|\mathcal{V}^{\mathtt{d}}|},$$

where $\bar{Z}_i$ is the value of variable Z_i in the solution of the ENDPPTC. First, we analyze the solutions according to these performance indicators and the network topologies and sizes. Second, we conduct sensitivity analyses on four parameters: the demand (b_i), the capacity of destination nodes (K_i), the number of lanes available for contraflow operations ($f_e^{\mathtt{M}}$), and the ratio between the free-flow speed and the backward wave speed (δ).

5.5.1 Analyses of network topology and size

Table 7 reports for every network structure (G, I, L, and S) and rectangular area, the average value of each performance indicator. We can notice that on average 66.8% and 33.2% of the total evacuation time are spent traveling and waiting. Additionally, the maximum time required for all the demand to be evacuated is on average 0.7 hour (approximately 45 minutes). Finally, 91.8% of the shelters are used in the solutions on average.

Table 7: Average values of the performance indicators according to the network topologies and sizes

		Evac. time	%Travel	%Waiting	Max evac. duration	%Shelter used
Topology						
Grid (G)		481.3	76.2	23.8	0.5	91.7
Irregular (I)		545.6	74.9	25.1	0.6	91.9
Grid-like (L)		549.3	71.9	28.1	0.7	92.4
Sparse (S)		790.3	52.0	48.0	1.0	91.4
Size						
$h \times w = 120$	6×20	1,230.8	71.1	28.9	0.9	84.9
	8×15	935.6	70.0	30.0	0.7	86.5
	10×12	842.7	72.5	27.5	0.7	86.5
$h \times w = 60$	4×15	649.5	59.3	40.7	0.9	86.5
	5×12	470.7	64.3	35.7	0.7	90.6
	6×10	518.7	61.7	38.3	0.7	91.7
$h \times w = 36$	3×12	239.0	63.1	36.9	0.6	100.0
	4×9	240.7	57.9	42.1	0.6	100.0
	6×6	197.2	60.1	39.9	0.5	100.0
Average		591.7	66.8	33.2	0.7	91.8

By analyzing the results according to the different network topologies, we realize that for grid (G), irregular (I), and grid-like (L) networks the average time spent waiting during the evacuation represents

less than 30% of the total evacuation time. In contrast, this is drastically different for sparse (S) networks where on average 48% of the evacuation time is spent waiting. We also note an increase in the average maximum evacuation duration in sparse networks. These results can be explained by the fact that these networks have less roads thus yielding more traffic, which in turn results in more waiting during the evacuation.

By analyzing the results according to the different network sizes, we can realize that for larger networks the average time spent traveling during the evacuation is higher than in smaller networks. More precisely, in networks with $h \times w = 120$, on average more than 70% of the total evacuation time is spent traveling, while in networks with $h \times w = \{36, 60\}$ it represents less than 65% of the total evacuation time. This can be explained by the fact the smaller network sizes have less potential paths for evacuation which creates more congestion, i.e., waiting. In addition, for a given network size, as the value of h/w increases, the average evacuation time tends to decrease. For example, with $h \times w = 120$, the average total evacuation time is 1,230.8, 935.6, and 842.7 hours with $h/w = 0.3$, $h/w = 0.53$, and $h/w = 0.83$. In fact, as the value of h/w increases, the source and destination nodes are usually closer which reduces the evacuation time. Finally, we can note that as the size of the network increases, less shelters are used. In our instances, this can be explained by the fact that there are more shelters in larger networks, which allows for a larger shelter capacity in proportion of the total demand.

5.5.2 Sensitivity analyses

In this section, we conduct sensitivity analyses to evaluate the impact on the performance indicators of four varying parameters **independently**: the demand (b_i), the destination node capacity (K_i), the number of lanes available for contraflow operations ($f_e^{\mathtt{M}}$), and the ratio between the free-flow speed and the backward wave speed (δ). Table 8 reports for each parameter change, the average percentage of increase for each performance indicator, denoted by Δ *Performance indicator*. To compute Δ *Performance indicator*, we first compute for each parameter change, each performance indicator and each instance the percentage of increase according to the initial value of the parameter. As an example, when increasing the demand from b_i to $2.5b_i$, the impact on the evacuation time is computed as $(z^*_{2.5b_i} - z^*_{b_i})/z^*_{b_i}$, where $z^*_{2.5b_i}$ and $z^*_{b_i}$ are the total evacuation times with $2.5b_i$ and b_i, and reported as a percentage. These values are then averaged over all the instances and reported in Table 8.

Table 8: Average percentage of increase in the performance indicators for the different sensitivity analyses

	Δ Evac. time (%)	Δ Travel (%)	Δ Waiting (%)	Δ Max evac. duration (%)	Δ Shelter used (%)
Demand (b_i)					
$1.5b_i$	80.5	–16.6	33.5	28.9	0.4
$2b_i$	181.8	–28.0	56.4	58.1	0.8
$2.5b_i$	303.4	–36.8	74.2	87.7	0.6
Shelter capacity (K_i)					
$\phi = 0.4$	–6.4	–3.0	6.1	–8.5	–27.3
$\phi = 0.2$	–8.1	–3.6	7.3	–10.6	–37.5
$\phi = 1/\mathtt{K}$	–8.4	–4.1	8.2	–11.2	–39.8
Number of lanes available for contraflow operations ($f_e^{\mathtt{M}}$)					
0	7.1	7.8	–9.1	24.1	0.4
Ratio between free-flow speed and backward wave speed (δ)					
0.2	0.6	–0.4	0.7	0.2	0.0
0.5	0.0	0.0	0.0	–0.1	0.0

First, when increasing the demand by 1.5, 2, and 2.5, the average total evacuation time increases by 80.5%, 181.8%, and 303.4%, and the maximum evacuation duration increases by 28.9%, 58.1%, and 87.7%. This is explained by the fact that the percentage of the total evacuation time spent waiting increases which is due to a more congested network. We can also note that increasing the demand has almost no impact on the number of shelters.

Second, we increased the destination node capacities (K_i). Recall that we had set $\phi = 0.8$ and

$$K_i = \frac{\sum_{k \in \mathcal{V}^{\mathtt{s}}} b_k}{\phi \cdot \mathtt{K}}, \forall i \in \mathcal{V}^{\mathtt{d}}.$$

In these sensitivity analyses, we set $\phi = \{0.4, 0.2, 1/\mathtt{K}\}$. Our results show that increasing the shelter capacity tends to decrease the total evacuation time as well as the maximum evacuation duration, but the effect is not linear. Doubling the shelter capacity ($\phi = 0.4$) decreases the evacuation time and the maximum evacuation duration by an average of 6.4% and 8.5%, while quadrupling the shelter capacity ($\phi = 0.2$) decreases these values by 8.1% and 10.6%. In addition, as expected, the percentage of shelters used decreases as their capacity increases. With $\phi = 0.4$ and $\phi = 0.2$, the average number of shelters used decreases by 27.3% and 37.5%. Finally, when the shelter capacity is equal to the total demand, i.e., by setting $\phi = 1/\mathtt{K}$, the total evacuation time and the maximum evacuation duration decrease by an average of 8.4% and 11.2%, and the percentage of shelters used decreases by 39.8%. This shows the need to have more than one shelter location even if the capacity of the shelters is not restricting, as this allows for more evacuation paths and reduces the total evacuation time and the maximum evacuation duration.

Third, we aim to assess the impact of allowing contraflow operations or not. Recall, that we had set $f_e^{\mathtt{M}} = f_e - 1, \forall e \in \mathcal{E} \setminus \mathcal{E}^p$. In these sensitivity analyses, we set $f_e^{\mathtt{M}} = 0, \forall e \in \mathcal{E} \setminus \mathcal{E}^p$. The results show that allowing contraflow operations allows to decrease the evacuation time and the maximum evacuation duration by an average of 7.1% and 24.1%. This is mostly explained by the fact that allowing contraflow operations reduces the time spent during an evacuation for waiting as it allows for more evacuation possibilities.

Fourth, we aim to determine the impact of the traffic congestion, represented by δ, on the solutions. In the literature, this value usually ranges from 0.2 to 0.5 (Zheng and Chiu, 2011). Therefore, we had set $\delta = 0.3$ and conduct sensitivity analyses by setting $\delta = \{0.2, 0.5\}$. Modifying the ratio between the free-flow speed and the backward wave speed has almost no impact on the total evacuation time and the maximum evacuation duration. When considering $\delta = 0.2$, which implies more traffic congestion, the total evacuation time and the maximum evacuation duration increase by 0.6% and 0.2%. This is due to higher waiting times caused by more traffic congestion. For our instances, the results with $\delta = 0.3$ and $\delta = 0.5$ are similar.

Our results show that the parameter with the most impact on traffic congestion is the demand. Therefore, estimating it is crucial when planning evacuations. In practice, if the demand is not evacuated simultaneously, which is the case in phased evacuation (Wolshon et al., 2006), this can mitigate the impact of wrongly estimating the demand. Our results also show that the parameter with the most impact on the percentage of shelter used is the capacity of shelters. Surprisingly, we can also see that more or less traffic congestion, represented by δ, has almost no impact on the evacuation time.

6 Conclusions

As disasters become increasingly frequent, effective evacuation planning has become crucial for protecting human lives. A key early decision during emergencies is determining whether evacuation is necessary, with the goal of relocating individuals to designated safety zones or shelters. These shelters, which provide protection for those displaced or at risk, must be accessible and strategically located outside of threatened areas. Additionally, transportation plans must be thoughtfully devised, taking potential traffic into account to ensure that evacuees can reach shelters both promptly and safely. Failure to consider traffic in evacuation planning can result in inaccurate evacuation time estimates and compromise the overall effectiveness of the response. Thus, key decisions in disaster preparedness include the strategic selection of shelter locations and the design of transportation plans that account for traffic—both essential components of an effective evacuation network.

In this study, we propose a new mathematical model that integrates traffic congestion and shelter location decisions. Traffic congestion is addressed through a CTM-based formulation that also

incorporates contraflow operations, time-variant road properties, multiple periods, and the definition of road capacities. Given that this integration leads to an intractable problem for real-size instances, we developed exact and heuristic solution methods based on Benders decomposition to solve it. To further enhance these methods, we proposed strategies such as the formulation of a stronger master problem. Additionally, we generated 144 problem instances with varying topologies and network sizes, inspired by real-world configurations. These instances are valuable to researchers, providing standardized datasets for those studying evacuation planning and enabling comparative analysis across different approaches.

The computational results demonstrate the effectiveness of the proposed solution strategies in efficiently solving the problem. The best exact method found optimal solutions for 94.4% of the tested instances, with an average optimality gap of less than 0.01%. Additionally, the results highlight that ignoring traffic congestion leads to a poor estimation of evacuation time, causing greater delays in evacuation operations. To mitigate the impact of traffic congestion, one effective strategy is to consider longer alternative routes for evacuation, which increases total travel time but reduces overall waiting time due to congestion. While this behavior was consistent across different network topologies, the impact of traffic congestion is more pronounced in sparse networks, which typically have fewer roads and, therefore, fewer options for diverting traffic.

Contraflow operations significantly impact total evacuation time, with a 7.1% increase observed when they were not implemented. Changes in evacuee demand also have a substantial effect, with doubling the demand leading to a 181.8% increase in total evacuation time. In this scenario, waiting time increased far more than travel time. Additionally, variations in shelter capacity impact the total evacuation time, though not directly proportional to changes in capacity. When shelters have large capacities, adding more shelters does not necessarily reduce evacuation time. Ignoring shelter capacity during planning can result in infeasible evacuation networks if the selected shelters cannot accommodate the actual demand. Therefore, accurately estimating evacuee demand and considering shelter capacity are crucial when planning evacuations under traffic congestion.

In conclusion, this study highlights the critical role of integrated planning in ensuring the efficiency and feasibility of evacuation strategies. By addressing multiple factors simultaneously, we provide a more realistic approach to evacuation planning. Future research could explore the application of this model in different real disaster scenarios and investigate the impact of real-time data on evacuation strategies, opening new avenues for dynamic and adaptive evacuation planning while considering different forms of uncertainty.

Declaration of generative AI and AI-assisted technologies in the writing process

During the preparation of this work the authors used ChatGPT in order to improve the readability and language of the manuscript. After using ChatGPT, the authors reviewed and edited the content as needed and takes full responsibility for the content of the published article.

Appendix

A Notation

Sets	
$\mathcal{V}$	Nodes
$\mathcal{V}^{\mathtt{s}}$	Source nodes, i.e., threatened or affected communities
$\mathcal{V}^{\mathtt{d}}$	Destination nodes, i.e., potential shelter locations
$\{p\}$	Super destination node/cell
$\mathcal{E}$	Directed links (roads)
$\mathcal{L}_e$	Set of lanes that can be used on a given link $e \in \mathcal{E} \setminus \mathcal{E}^p$ (including lanes for contraflow operations)
T^τ	Set of periods in the time horizon
$\mathcal{C}$	Set of cells
$\mathcal{C}_e$	Set of cells that belongs to link $e \in \mathcal{E} \setminus \mathcal{E}^p$
$\mathcal{C}^{\mathtt{s}}$	Source cells, i.e., cells representing sources nodes
$\mathcal{C}^{\mathtt{d}}$	Destination cells, i.e., cells representing destination nodes
Γ_j	Successors cells of cell $j \in \mathcal{C}$
Γ_j^{-1}	Predecessor cells of cell $j \in \mathcal{C}$
Parameters	
b_i	Demand in source node $i \in \mathcal{V}^{\mathtt{s}}$
K_i	Capacity of shelter $i \in p$
$m^{\mathtt{d}}$	Minimum number of vehicles that can be sent to the shelters during evacuation operations
$m^{\mathtt{e}}$	Minimum number of vehicles that can be sent over the links during evacuation operations
f_e	Number of lanes available in link $e \in \mathcal{E}$
$f_e^{\mathtt{M}}$	Maximum number of lanes that can be used for contraflow operations in link $e \in \mathcal{E}$
E	Maximum number of links in which contraflow operations can be defined
K	Maximum number of shelters that can be operated
N_{ilt}	Maximum number of vehicles that can be accommodated in cell $i \in \mathcal{C}$ at time interval $t \in T$ given l lanes in operation
Q_{ilt}	Maximum number of vehicles that can pass in/out of cell $i \in \mathcal{C}$ during time interval $t \in T$ given l lanes in operation
n_{ji}	Binary parameter equal to 1 if node $i \in \mathcal{V} \setminus \mathcal{V}^{\mathtt{u}}$ in graph G is represented by cell $j \in \mathcal{C} \setminus \cup_{e \in \mathcal{E}} \mathcal{C}_e$ in the cell-representation graph G^τ, and 0 otherwise
$g_{ee'}$	Binary parameter equal to 1 if links $e \in \mathcal{E} \setminus \mathcal{E}^p$ and $e' \in \mathcal{E} \setminus \mathcal{E}^p$ represent the same road in opposite directions, and 0 otherwise
τ	Discrete size of the time steps
δ	Ratio $\frac{w}{u}$ (u and w are the free-flow and backward wave speed)
Decision variables	
Z_i	Binary variable equal to 1 if shelter $i \in p$ is opened, and 0 otherwise
L_{le}	Binary variable equal to 1 if l lanes are selected for operation in link $e \in \mathcal{E}$, and 0 otherwise
X_{jt}	Number of vehicles in cell $j \in \mathcal{C}$ at period $t \in T^\tau$
Y_{jkt}	Number of vehicles moving from cell $j \in \mathcal{C}$ to cell $k \in \Gamma_j$ at period $t \in T^\tau$

B Instance generation

In this section, we provide additional details on the generated instances. First, we provide the algorithm that we implemented to generate the different categories of roads (freeway, arterial street and local street). Second, we give an overview of the characteristics of the generated instances.

B.1 Algorithm to generate the different type of roads

Given the number of freeways and arterial streets, these roads are built using an algorithm based on shortest path problems. For instance, a basic scheme for the construction of freeways from left to right is outlined in Algorithm A1. The same procedure is repeated to generate the arterial streets from left to right and also for freeways and arterial streets from bottom to top. We first generate the freeways and then the arterial streets. Once an arc belong to a freeway, we do not consider it for the generation of arterial streets. Finally, after the generation of freeways and arterial streets, the reaming arcs are considered belonging to local streets.

Algorithm A1 Basic scheme for the construction of freeways from left to right

1: `Initialization`:
   Let F be the number of freeways from left to right.
   Let (x_i, y_i) be coordinates indicating the location of node i.
   Let h and w be the height and width of the network, respectively.
   Set $dist = \frac{\text{height}}{F}$.
2: Divide the network from bottom to top in F sections of length $dist$.
3: **for** $f = 1$ **to** F **do**
4: Randomly select a node i such that $x_i \leq 1$ (on the left) and $(f-1) \cdot dist \leq y_i \leq f \cdot dist$ (in section f);
5: Randomly select a node j such that $x_j \geq w - 1$ (on the right) and $(f-1) \cdot dist \leq y_j \leq f \cdot dist$ (in section f);
6: Find the shortest path $i - j$ from node i to node j;
7: Set the arcs in the shortest path $i - j$ as arcs that belong to freeway f;
8: **end for**

B.2 Characteristic of the generated instances

Table A1 shows the main characteristics of the generated networks: the topology, the size, the ratio $(\frac{\text{h}}{\text{w}})$, the average degree ¡k¿, the number of nodes, the number of source and destination nodes, the node positioning, the shelter location, the number of arcs, the arc length, the minimal distance between the source and destination nodes and the number of generated networks.

Table A1: Characteristics of the randomly generated networks

Topology	Size ($h \times w$)	Ratio ($\frac{h}{w}$)	¡k¿	#nodes	$\lvert\mathcal{V}^{\mathrm{s}}\rvert$	$\lvert\mathcal{V}^{\mathrm{d}}\rvert$	Node positioning*	Shelter location*	#arcs	Arc length	Min dist. $S-D$**	# networks
Grid (G)	6×20	0.26	1.78	120	8	12	E	A, S	214	$r = 1$	$d = 3, 5$	4
Grid (G)	8X15	0.50	1.81	120	8	12	E	A, S	217	$r = 1$	$d = 3, 5$	4
Grid (G)	10X12	0.82	1.82	120	8	12	E	A, S	218	$r = 1$	$d = 3, 5$	4
Grid-like (L)	6X20	0.26	1.78	120	8	12	E	A, S	214	$r \leq 2$	$d = 3, 5$	4
Grid-like (L)	8X15	0.50	1.81	120	8	12	E	A, S	217	$r \leq 2$	$d = 3, 5$	4
Grid-like (L)	10X12	0.82	1.82	120	8	12	E	A, S	218	$r \leq 2$	$d = 3, 5$	4
Irregular (I)	6X20	0.26	1.78	120	8	12	R	A, S	214	$r \leq 2$	$d = 3, 5$	4
Irregular (I)	8X15	0.50	1.81	120	8	12	R	A, S	217	$r \leq 2$	$d = 3, 5$	4
Irregular (I)	10X12	0.82	1.82	120	8	12	R	A, S	218	$r \leq 2$	$d = 3, 5$	4
Sparse (S)	6X20	0.26	1.79	48	8	12	R	A, S	86	$r \leq 2$	$d = 3, 5$	4
Sparse (S)	8X15	0.50	1.81	48	8	12	R	A, S	87	$r \leq 2$	$d = 3, 5$	4
Sparse (S)	10X12	0.82	1.83	48	8	12	R	A, S	88	$r \leq 2$	$d = 3, 5$	4
Grid (G)	4X15	0.21	1.68	60	4	6	E	A, S	101	$r = 1$	$d = 3, 5$	4
Grid (G)	5X12	0.36	1.72	60	4	6	E	A, S	103	$r = 1$	$d = 3, 5$	4
Grid (G)	6X10	0.56	1.73	60	4	6	E	A, S	104	$r = 1$	$d = 3, 5$	4
Grid-like (L)	4X15	0.21	1.68	60	4	6	E	A, S	101	$r \leq 2$	$d = 3, 5$	4
Grid-like (L)	5X12	0.36	1.72	60	4	6	E	A, S	103	$r \leq 2$	$d = 3, 5$	4
Grid-like (L)	6X10	0.56	1.73	60	4	6	E	A, S	104	$r \leq 2$	$d = 3, 5$	4
Irregular (I)	4X15	0.21	1.68	60	4	6	R	A, S	101	$r \leq 2$	$d = 3, 5$	4
Irregular (I)	5X12	0.36	1.72	60	4	6	R	A, S	103	$r \leq 2$	$d = 3, 5$	4
Irregular (I)	6X10	0.56	1.73	60	4	6	R	A, S	104	$r \leq 2$	$d = 3, 5$	4
Sparse (S)	4X15	0.21	1.71	24	4	6	R	A, S	41	$r \leq 2$	$d = 3, 5$	4
Sparse (S)	5X12	0.36	1.75	24	4	6	R	A, S	42	$r \leq 2$	$d = 3, 5$	4
Sparse (S)	6X10	0.56	1.75	24	4	6	R	A, S	42	$r \leq 2$	$d = 3, 5$	4
Grid (G)	3X12	0.18	1.58	36	2	3	E	A, S	57	$r = 1$	$d = 3, 5$	4
Grid (G)	4X9	0.38	1.64	36	2	3	E	A, S	59	$r = 1$	$d = 3, 5$	4
Grid (G)	6X6	1.00	1.67	36	2	3	E	A, S	60	$r = 1$	$d = 3, 4$	4
Grid-like (L)	3X12	0.18	1.58	36	2	3	E	A, S	57	$r \leq 2$	$d = 3, 5$	4
Grid-like (L)	4X9	0.38	1.64	36	2	3	E	A, S	59	$r \leq 2$	$d = 3, 5$	4
Grid-like (L)	6X6	1.00	1.67	36	2	3	E	A, S	60	$r \leq 2$	$d = 3, 4$	4
Irregular (I)	3X12	0.18	1.58	36	2	3	R	A, S	57	$r \leq 2$	$d = 3, 5$	4
Irregular (I)	4X9	0.38	1.64	36	2	3	R	A, S	59	$r \leq 2$	$d = 3, 5$	4
Irregular (I)	6X6	1.00	1.67	36	2	3	R	A, S	60	$r \leq 2$	$d = 3, 4$	4
Sparse (S)	3X12	0.18	1.53	15	2	3	R	A, S	23	$r \leq 2$	$d = 3, 5$	4
Sparse (S)	4X9	0.38	1.60	15	2	3	R	A, S	24	$r \leq 2$	$d = 3, 5$	4
Sparse (S)	6X6	1.00	1.60	15	2	3	R	A, S	24	$r \leq 2$	$d = 3, 4$	4

* E: equidistant; R: random; S: surrounding; A: aside.
** Minimum distance from sources to shelters.

C Proposed benchmarks

In this section, we present a description of the proposed benchmark approaches (FLA and BPR). These benchmarks are used to verify the impact of traffic congestion into the problem.

C.1 Flow location-allocation model (ENDPP)

$ENDPP$ is a flow location-allocation problem in which no traffic congestion is considered. The sets, parameters, and variables for the $ENDPP$ are defined as follows.

Sets	
$\mathcal{V}$	Nodes
$\mathcal{V}^{\mathrm{s}}$	Source nodes, i.e., threatened or affected communities
$\mathcal{V}^{\mathrm{d}}$	Destination nodes, i.e., potential shelter locations
p	Super destination node
$\mathcal{E}$	Directed links (streets)
$\mathcal{E}_i$	Set of arcs incident to node $i \in \mathcal{V}$
$\mathcal{E}_i^-$	Set of incoming arcs for node $i \in \mathcal{V}$
$\mathcal{E}_i^+$	Set of outgoing arcs for node $i \in \mathcal{V}$

Parameters	
τ	Discrete size of the time steps
$\ell_e = \lvert C_e \rvert$	Travel time in link $e \in \mathcal{E}$ (in number of periods)
K_i	Capacity of shelter $i \in \mathcal{V}^{\mathtt{d}}$
U_e	Practical capacity of the link $e \in \mathcal{E}$ (maximum flow rate, in vehicles per hour)
Additional variables	
X_e	Flow of vehicles on arc $e \in \mathcal{E}$
Z_i	Binary variable equal to 1 if shelter $i \in \mathcal{V}^{\mathtt{d}}$ is used for the evacuation operations, and 0 otherwise.
L_{le}	Binary variable equal to 1 if l lanes are selected for operation in link $e \in \mathcal{E}$, and 0 otherwise.

Based on the above notation, the $ENDPP$ problem is stated as follows.

$$(ENDPP) \quad \min \sum_{e \in \mathcal{E}} \tau \ell_e X_e, \tag{A1}$$

s.t.

$$\sum_{e \in \mathcal{E}_i^+} X_e = d_i, \qquad \forall\, i \in \mathcal{V}^{\mathtt{s}}, \tag{A2}$$

$$\sum_{e \in \mathcal{E}_p^-} X_e = \sum_{i \in \mathcal{V}^{\mathtt{s}}} b_i, \tag{A3}$$

$$\sum_{e \in \mathcal{E}_i^+} X_e = \sum_{e \in \mathcal{E}_i^-} X_e, \qquad \forall\, i \in \mathcal{V} \setminus \{\mathcal{V}^{\mathtt{s}}, \{p\}\}, \tag{A4}$$

$$X_e \geq m^{\mathtt{e}} \sum_{l \in \mathcal{L}_e} L_{le}, \qquad \forall\, e \in \mathcal{E}, \tag{A5}$$

$$X_e \geq m^{\mathtt{d}} Z_i, \qquad \forall\, e \in \{\mathcal{E}_i^+ \cup \mathcal{E}_p^-\}, i \in \mathcal{V}^{\mathtt{d}}, \tag{A6}$$

$$X_e \leq K_i Z_i, \qquad \forall\, e \in \{\mathcal{E}_i^+ \cup \mathcal{E}_p^-\}, i \in \mathcal{V}^{\mathtt{d}}, \tag{A7}$$

$$X_e \leq \sum_{l \in \mathcal{L}_e} U_e L_{le}, \tag{A8}$$

$$\sum_{i \in \mathcal{V}^{\mathtt{d}}} Z_i \leq K, \tag{A9}$$

$$\sum_{l \in \mathcal{L}_e} L_{le} + \sum_{l \in \mathcal{L}_{e'}} L_{le'} \leq 1, \qquad \forall\, e \in \mathcal{E}, e' \in \mathcal{E} : r_{ee'} = 1, \tag{A10}$$

$$\sum_{l \in \mathcal{L}_e} l L_{le} \leq f_e + f_{e'}^{\mathtt{M}}, \qquad \forall\, e \in \mathcal{E}, e' \in \mathcal{E} : r_{ee'} = 1, \tag{A11}$$

$$\sum_{e \in \mathcal{E}} \sum_{l \in \mathcal{L}_e : l > f_e} L_{le} \leq E, \tag{A12}$$

$$Z_i \in \{0,1\}, L_{le} \in \{0,1\}, \qquad \forall\, i \in \mathcal{V}^{\mathtt{d}}, l \in \mathcal{L}_e, e \in \mathcal{E}, \tag{A13}$$

$$X_e \geq 0, \qquad \forall\, e \in \mathcal{E}. \tag{A14}$$

Constraints (A2) set the flow of vehicles in the source nodes. Constraints (A3) set the flow of vehicles in the super sink node, while constraints (A4) set the flow of vehicles in the other nodes of the network. Constraints (A5) and (A6) establish the minimum flow in arcs and shelters to consider its operation. Constraints (A7) set the capacity limit in the shelters, while constraints (A8) set the capacity limit for arcs. Constraint (A9) limits the number of shelters that can be opened. Constraints (A10) force the evacuation flow to only one direction in a given street segment. Constraints (A11) limit the number of lanes that can be used in the evacuation operations to the number of available lanes. Constraints (A12) set a limit on the number of links with contraflow operations. Finally, constraints (A13) and (A14) establish the domain of the decision variables.

C.2 Flow location-allocation model with BPR function (EPPTC-BPR)

EPPTC-BPR is the *EPP* model using the BPR function to approximate traffic in a single period context.

$$\text{(EPPTC-BPR)} \quad \min \sum_{e\in\mathcal{E}} \tau \ell_e X_e \left(1+\alpha\left(\frac{X_e}{U_e}\right)^{\beta}\right),$$

s.t.

Constraints (A2)–(A14).

where U_e is the practical capacity of the link $e \in \mathcal{E}$ (maximum flow rate, in vehicles per hour), the parameters $\alpha \geq 0$ and $\beta \geq 0$ reflect the road characteristics, and they are taken as 0.15 and 4, respectively. The problem is linearized using a piecewise linear approximation (Afkham et al., 2022).

D Matheuristic BBC

In this section, we present a matheuristic BBC algorithm to solve the EPPTC. In what follows, we describe the proposed matheuristic and present some computational results.

D.1 Matheuristic descripticion

In the proposed BBC algorithm, solving the subproblem is non-trivial and requires most of the computational time. Therefore, we have implemented a matheuristic BBC algorithm which relies on solving the subproblem heuristically. Note that the MP is formulated with Model (2) (see Section 4.1.1), but the optimality and feasibility cuts have to be adapted due to the changes in the SP. In addition, a different time step $\gamma \geq \tau$ can be defined for the master problem, i.e., the master problem solution for τ is approximated using time step γ.

The matheuristic BBC consists of solving the SP heuristically by solving several auxiliary subproblems in an iterative manner. Each auxiliary subproblem, referred to as SP_h, is similar to the exact SP using Model (3), but solved over a subset $h \leq |T^\tau|$ of time periods by considering a penalty in the objective function and heuristic lower and upper bounds for variables Y_{jkt} and X_{jt}. More precisely, rather than including constraints (1q), the objective function of SP_h considers a penalty to be minimized when the demand is not fully evacuated.

We provide a detailed mathematical formulation for auxiliary subproblem SP_h, with $h \leq |T^\tau|$. Let us recall that $\bar{Y}^{\texttt{lw}}_{jkth}$ and $\bar{Y}^{\texttt{up}}_{jkth}$ are predefined lower and upper bounds for variable Y_{jkt}, while $\bar{X}^{\texttt{lw}}_{jth}$ and $\bar{X}^{\texttt{up}}_{jth}$ are predefined lower and upper bounds for variable X_{jt}. Also, let $\bar{Y}^{\gamma}_{et}$ be the solution of variable Y^{γ}_{et} in the master problem MP*. For a given h, its corresponding auxiliary subproblem SP_h can then be modeled as follows:

$$\min \quad \sum_{j\in\mathcal{C}\setminus\{p\}} \tau|T^\tau|X_{jh} + \sum_{j\in\mathcal{C}^{\text{d}}} \sum_{\substack{t\in T^\tau:\\ t\leq h}} \tau t Y_{jpt} \quad - \sum_{j\in\mathcal{C}} \sum_{k\in\mathcal{C}\setminus\{p\}} \sum_{\substack{t\in T^\tau:\\ t\leq h}} \tau|T^\tau|Y_{jkt} \tag{A15a}$$

$$\text{s.t.} \quad X_{j1} = b_i + X_{j0} - \sum_{k\in\Gamma_j} Y_{jk0}, \quad \forall\, j \in \mathcal{C}^{\text{s}},\ i \in \mathcal{V}^{\text{s}} : n_{ji} = 1, \tag{A15b}$$

$$X_{jt} = X_{j(t-1)} - \sum_{k\in\Gamma_j} Y_{jk(t-1)}, \quad \forall\, j \in \mathcal{C}^{\text{s}}, t \in T^\tau : 1 < t \leq h, \tag{A15c}$$

$$X_{pt} = X_{p(t-1)} + \sum_{k\in\Gamma_p^{-1}} Y_{kp(t-1)}, \quad \forall\, t \in T^\tau : t \leq h, \tag{A15d}$$

$$X_{jt} = X_{j(t-1)} + \sum_{k\in\Gamma_j^{-1}} Y_{kj(t-1)} - \sum_{k\in\Gamma_j} Y_{jk(t-1)}, \quad \forall\, j \in \mathcal{C}\setminus\{\mathcal{C}^{\text{s}}\cup\{p\}\}, t \in T^\tau : t \leq h, \tag{A15e}$$

$$\sum_{k\in\Gamma_j} Y_{jkt} \leq X_{jt}, \quad \forall\, j \in \mathcal{C}\setminus\{p\}, t \in T^\tau : t \leq h, \tag{A15f}$$

$$\sum_{k\in\Gamma_j} Y_{jkt} \leq \sum_{l\in\mathcal{L}_e} Q_{jlt}\bar{L}_{le}, \quad \forall\, j \in \mathcal{C}_e, e \in \mathcal{E}, t \in T^\tau : t \leq h, \tag{A15g}$$

$$\sum_{j\in\Gamma_k^{-1}} Y_{jkt} \leq \sum_{l\in\mathcal{L}_e} Q_{klt}\bar{L}_{le}, \quad \forall\, k \in \mathcal{C}_e, e \in \mathcal{E}, t \in T^\tau : t \leq h, \tag{A15h}$$

$$\sum_{j\in\Gamma_k^{-1}} Y_{jkt} + \delta X_{kt} \leq \sum_{l\in\mathcal{L}_e} \delta N_{klt}\bar{L}_{le}, \quad \forall\, k \in \mathcal{C}_e, e \in \mathcal{E}, t \in T^\tau : t \leq h, \tag{A15i}$$

$$\sum_{\substack{t\in T^\tau:\\ t\leq h}} Y_{jpt} \leq k_i^{\mathtt{d}}\bar{Z}_i, \quad \forall\, j \in \mathcal{C}^{\mathtt{d}},\ i \in \mathcal{V}^{\mathtt{d}} : n_{ji} = 1, \tag{A15j}$$

$$\sum_{\substack{t\in T^\tau:\\ t\leq h}} \sum_{j\in\Gamma_k^{-1}} Y_{jkt} \leq \sum_{t\in T^\tau} \bar{Y}^{\gamma}_{et}, \quad \forall\, k \in \mathcal{C}_e, e \in \mathcal{E}, \tag{A15k}$$

$$\bar{Y}^{\mathtt{lw}}_{jkth} \leq Y_{jkt} \leq \bar{Y}^{\mathtt{up}}_{jkth}, \quad \forall\, j \in \mathcal{C},\ k \in \Gamma_j, t \in T^\tau : t \leq h, \tag{A15l}$$

$$\bar{X}^{\mathtt{lw}}_{jth} \leq X_{jt} \leq \bar{X}^{\mathtt{up}}_{jth}, \quad \forall\, j \in \mathcal{C}, t \in T^\tau : t \leq h, \tag{A15m}$$

$$X_{jt} \geq 0,\ Y_{jkt} \geq 0, \quad \forall\, j \in \mathcal{C},\ k \in \Gamma_j, t \in T^\tau. \tag{A15n}$$

The first term of the objective function (A15a) penalizes the demand that is not evacuated until period h. The second term of the objective function (A15a) computes the total evacuation time for the demand that arrives at the shelters. Finally, the third term of the objective function (A15a) is employed to influence the progress of the demand that cannot be evacuated until period h toward shelters. Constraints (A15b)–(A15f) are equivalent to constraints (1b)–(1f). Constraints (A15g)–(A15j) are equivalent to constraints (3b)–(3e). Constraints (A15k) set a limit for the flow on links based on the solution $\bar{Y}^{\gamma}_{et}$ of the flow variable Y^{γ}_{et} from MIP*. These constraints ensure that the original minimum flow constraints (3f) and (3g) are met, since the flow in MIP* satisfy them. Finally, constraints (A15l) and (A15m) set bounds for variables Y_{jkt} and X_{jt}.

The initial value of h is determined such that the evacuated demand is positive, and the lower bounds for variables X_{jt} and Y_{jkt} are set to 0, while their corresponding upper bounds are set to infinity. Then, at each iteration, the value of h is incremented by $\mathtt{ts}$, and the bounds for variables Y_{jkt} and X_{jt} are modified depending on the optimal solution obtained in the previous iteration denoted by $\bar{Y}_{jkt}$ and $\bar{X}_{jt}$. That is, for a given subproblem SP$_h$, let us denote by $\bar{Y}^{\mathtt{lw}}_{jkth}$ and $\bar{Y}^{\mathtt{up}}_{jkth}$ the lower and upper bounds for variable Y_{jkt}, and $\bar{X}^{\mathtt{lw}}_{jth}$ and $\bar{X}^{\mathtt{up}}_{jth}$ the lower and upper bounds for variable X_{jt}. Using the optimal solution obtained at the previous iteration, $\bar{Y}_{jkt}$ and $\bar{X}_{jt}$, these bounds are set as $\bar{Y}^{\mathtt{lw}}_{jkth} = \bar{Y}^{\mathtt{up}}_{jkth} = \bar{Y}_{jkt}$, and $\bar{X}^{\mathtt{lw}}_{jth} = \bar{X}^{\mathtt{up}}_{jth} = \bar{X}_{jt}$. Because h only considers a subset of time periods, this implies that only a portion of the total demand might be evacuated. Therefore, this process is repeated until the total demand is evacuated. Algorithm A2 provides a pseudo-code of this process to solve SP heuristically. Note that even though SP$_h$ is easier to solve than the exact SP, because several auxiliary subproblems SP$_h$ may have to be solved this process can be computationally extensive.

When the subproblem is solved heuristically, the optimality and feasibility cuts as defined in Equations (4) and (5) cannot be generated. Instead, new optimality and feasibility cuts are defined. Let $\tilde{\Theta}$ be computed by evaluating the solution from the last solved subproblem SP$_h$, where all the population has been evacuated, according to the original objective function (3a). The optimality cuts are then defined as:

$$\Theta \geq \tilde{\Theta} + \tilde{\Theta}\Bigg(\sum_{\substack{i\in\mathcal{V}^{\mathtt{d}}:\\ \tilde{Z}_i=1}} (Z_i - 1) - \sum_{\substack{i\in\mathcal{V}^{\mathtt{d}}:\\ \tilde{Z}_i=0}} Z_i + \sum_{e\in\mathcal{E}\setminus\mathcal{E}^p} \sum_{\substack{l\in\mathcal{L}_e:\\ \tilde{L}_{le}=1}} (L_{le} - 1) - \sum_{e\in\mathcal{E}\setminus\mathcal{E}^p} \sum_{\substack{l\in\mathcal{L}_e:\\ \tilde{L}_{le}=0}} L_{le}\Bigg). \tag{A16}$$

Similarly, the feasibility cuts are defined as:

$$\sum_{\substack{i\in\mathcal{V}^{\mathrm{d}}:\\ \bar{Z}_i=1}}(Z_i-1)-\sum_{\substack{i\in\mathcal{V}^{\mathrm{d}}:\\ \bar{Z}_i=0}}Z_i+\sum_{e\in\mathcal{E}\setminus\mathcal{E}^p}\sum_{\substack{l\in\mathcal{L}_e:\\ \bar{L}_{le}=1}}(L_{le}-1)-\sum_{e\in\mathcal{E}\setminus\mathcal{E}^p}\sum_{\substack{l\in\mathcal{L}_e:\\ \bar{L}_{le}=0}}L_{le}<0. \tag{A17}$$

Algorithm A2 Pseudo-code to solve the SP heuristically

Initialization: $h=\mathtt{sv}$, $\mathtt{Evacuated\_demand}=0$, $\mathtt{Total\_demand}=\sum_{i\in\mathcal{V}^{\mathrm{s}}}b_i$;
for $l=0$ **to** sv **do**
  $\bar{Y}^{\mathtt{lw}}_{jktl}=0$, $\bar{Y}^{\mathtt{up}}_{jktl}=\infty$, $\bar{X}^{\mathtt{lw}}_{jtl}=0$, $\bar{X}^{\mathtt{up}}_{jtl}=\infty$.
end for
while Evacuated_demand ¡ Total_demand **do**
  Solve SP_h;
  $\mathtt{Evacuated\_demand}=\sum_{j\in\mathcal{C}^{\mathrm{d}}}\sum_{\substack{t\in T^{\tau}:\\ t\le h}}\bar{Y}_{jpt}$;
  if $\mathtt{Evacuated\_demand}>0$ **then**
    for $l=0$ **to** h **do**
      $\bar{Y}^{\mathtt{lw}}_{jktl}=\bar{Y}_{jkt}$, $\bar{Y}^{\mathtt{up}}_{jktl}=\bar{Y}_{jkt}$, $\bar{X}^{\mathtt{lw}}_{jtl}=\bar{X}_{jt}$, $\bar{X}^{\mathtt{up}}_{jtl}=\bar{X}_{jt}$;
    end for
    for $l=h+1$ **to** $h+\mathtt{ts}$ **do**
      $\bar{Y}^{\mathtt{lw}}_{jktl}=0$, $\bar{Y}^{\mathtt{up}}_{jktl}=\infty$, $\bar{X}^{\mathtt{lw}}_{jtl}=0$, $\bar{X}^{\mathtt{up}}_{jtl}=\infty$;
    end for
    $h:=h+\mathtt{ts}$;
  else
    $\mathtt{sv}:=h+\mathtt{ts}$;
    for $l=h+1$ **to** sv **do**
      $\bar{Y}^{\mathtt{lw}}_{jktl}=0$, $\bar{Y}^{\mathtt{up}}_{jktl}=\infty$, $\bar{X}^{\mathtt{lw}}_{jtl}=0$, $\bar{X}^{\mathtt{up}}_{jtl}=\infty$;
    end for
    $h:=\mathtt{sv}$;
  end if
end while

Note. start value (sv) and time sloop (ts) are user-defined parameters for the initial value of h and its successive increments.

D.2 Results of the BBC matheuristic

The average computational results of the matheuristic over the tested instances with different time steps (τ) values are presented in Table A2, which reports the percentage of feasible solutions (%Feas), the average gap to the best upper bound obtained with the exact BBC, and the runtime (seconds). Notice that the matheuristic has the advantage of finding feasible solutions for all tested τ values, although it can be time-consuming in some cases, particularly for small time steps. In relation to the quality of the solutions, the heuristic finds solutions that, on average, are within 3% of the best solution obtained with the exact BBC.

Table A2: Average computational results of the BBC matheuristic for different time steps (τ)

τ	%Feas	Ratio	Seconds
6	100	1.79	8,796
9	100	1.25	8,214
12	100	1.07	6,619
15	100	1.04	6,458
18	100	2.22	6,394
21	100	1.26	4,440
24	100	0.97	3,502
27	100	1.16	3,049
30	100	2.21	1,370

References

Afkham, M., Ramezanian, R., and Shahparvari, S. (2022). Balancing traffic flow in the congested mass self-evacuation dynamic network under tight preparation budget: An Australian bushfire practice. Omega, 111:102658.

Alam, M. J. and Habib, M. A. (2021a). A dynamic programming optimization for traffic microsimulation modelling of a mass evacuation. Transportation Research Part D: Transport and Environment, 97(July):102946.

Alam, M. J. and Habib, M. A. (2021b). Mass evacuation microsimulation modeling considering traffic disruptions. Natural Hazards, 108(1):323–346.

Bayram, V. (2016). Optimization models for large scale network evacuation planning and management: A literature review. Surveys in Operations Research and Management Science, 21(2):63–84.

Bayram, V., Tansel, B. T., and Yaman, H. (2015). Compromising system and user interests in shelter location and evacuation planning. Transportation Research Part B: Methodological, 72:146–163.

Bayram, V. and Yaman, H. (2018a). A stochastic programming approach for Shelter location and evacuation planning. RAIRO - Operations Research, 52(3):779–805.

Bayram, V. and Yaman, H. (2018b). Shelter location and evacuation route assignment under uncertainty: A benders decomposition approach. Transportation Science, 52(2):416–436.

Bayram, V. and Yaman, H. (2024). A joint demand and supply management approach to large scale urban evacuation planning: Evacuate or shelter-in-place, staging and dynamic resource allocation. European Journal of Operational Research, 313(1):171–191.

Benders, J. (1962). Partitioning procedures for solving mixed-variables programming problems. Numerische Mathematik, 4(1):238–252.

Bish, D. R. and Sherali, H. D. (2013). Aggregate-level demand management in evacuation planning. European Journal of Operational Research, 224(1):79–92.

Bureau of Public Roads (1964). Traffic assignment manual: for application with a large, high speed computer. U.S. Department of Commerce, Washington, DC.

Christianson, A. C. and McGee, T. K. (2019). Wildfire evacuation experiences of band members of Whitefish Lake First Nation 459, Alberta, Canada. Natural Hazards, 98(1):9–29.

Coutinho-Rodrigues, J., Tralhão, L., and Alçada-Almeida, L. (2012). Solving a location-routing problem with a multiobjective approach: The design of urban evacuation plans. Journal of Transport Geography, 22:206–218.

Daganzo, C. F. (1994). The cell transmission model: A dynamic representation of highway traffic consistent with the hydrodynamic theory. Transportation Research Part B: Methodological, 28(4):269–287.

Daganzo, C. F. (1995). The cell transmission model, part II: Network traffic. Transportation Research Part B: Methodological, 29(2):79–93.

Dönmez, Z., Kara, B. Y., Karsu, Ö., and Saldanha-da Gama, F. (2021). Humanitarian facility location under uncertainty: Critical review and future prospects. Omega, 102:102393.

Dulebenets, M. A., Pasha, J., Abioye, O. F., Kavoosi, M., Ozguven, E. E., Moses, R., Boot, W. R., and Sando, T. (2019). Exact and heuristic solution algorithms for efficient emergency evacuation in areas with vulnerable populations. International Journal of Disaster Risk Reduction, 39:101114.

EM-DAT (2022). The international disaster database. Accessed on 01/12/2022.

Errico, F., Crainic, T. G., Malucelli, F., and Nonato, M. (2017). A benders decomposition approach for the symmetric TSP with generalized latency arising in the design of semiflexible transit systems. Transportation Science, 51(2):706–722.

Esposito Amideo, A., Scaparra, M. P., and Kotiadis, K. (2019). Optimising shelter location and evacuation routing operations: The critical issues. European Journal of Operational Research, 279(2):279–295.

Esposito Amideo, A., Scaparra, M. P., Sforza, A., and Sterle, C. (2021). An integrated user-system approach for shelter location and evacuation routing. Networks, 78(1):46–68.

Gendron, B., Scutellà, M. G., Garroppo, R. G., Nencioni, G., and Tavanti, L. (2016). A branch-and-Benders-cut method for nonlinear power design in green wireless local area networks. European Journal of Operational Research, 255(1):151–162.

Goerigk, M., Deghdak, K., and Heßler, P. (2014). A comprehensive evacuation planning model and genetic solution algorithm. Transportation Research Part E: Logistics and Transportation Review, 71:82–97.

Gouveia, L., Joyce-Moniz, M., and Leitner, M. (2018). Branch-and-cut methods for the Network Design Problem with Vulnerability Constraints. Computers and Operations Research, 91:190–208.

Hadas, Y. and Laor, A. (2013). Network design model with evacuation constraints. Transportation research part A: policy and practice, 47:1–9.

He, X., Zheng, H., Peeta, S., and Li, Y. (2018). Network Design Model to Integrate Shelter Assignment with Contraflow Operations in Emergency Evacuation Planning. Networks and Spatial Economics, 18(4):1027–1050.

Hessami, A. R., Faghihi, V., Kim, A., and Ford, D. N. (2020). Evaluating planning strategies for prioritizing projects in sustainability improvement programs. Construction Management and Economics, 38(8):726–738.

Hsiao, C.-C., Sun, M.-C., Chen, A. Y., and Hsu, Y.-T. (2021). Location problems for shelter-in-place deployment: A case study of vertical evacuation upon dam-break floods. International Journal of Disaster Risk Reduction, 57(December 2020):102048.

Insani, N., Akman, D., Taheri, S., and Hearne, J. (2022). Short-notice flood evacuation plan under dynamic demand in high populated areas. International Journal of Disaster Risk Reduction, 74(February):102844.

Jha, M., Moore, K., and Pashaie, B. (2004). Emergency Evacuation Planning with Microscopic Traffic Simulation. Transportation Research Record: Journal of the Transportation Research Board, 1886(1):40–48.

Kim, S., Shekhar, S., and Min, M. (2008). Contraflow transportation network reconfiguration for evacuation route planning. IEEE transactions on Knowledge and Data Engineering, 20(8):1115–1129.

Kimms, A. and Maassen, K. C. (2012a). A fast heuristic approach for large-scale cell-transmission-based evacuation route planning. Networks, 60(3):179–193.

Kimms, A. and Maassen, K. C. (2012b). Cell-transmission-based evacuation planning with rescue teams. Journal of Heuristics, 18(3):435–471.

Kongsomsaksakul, S., Yang, C., and Chen, A. (2005). Shelter location-allocation model for flood evacuation planning. Journal of the Eastern Asia Society for Transportation Studies, 6(1981):4237–4252.

Kulshrestha, A., Wu, D., Lou, Y., and Yin, Y. (2011). Robust Shelter Locations for Evacuation Planning with Demand Uncertainty. Journal of Transportation Safety and Security, 3(4):272–288.

Li, A. C., Nozick, L., Xu, N., and Davidson, R. (2012). Shelter location and transportation planning under hurricane conditions. Transportation Research Part E: Logistics and Transportation Review, 48(4):715–729.

Li, Y., Waller, S. T., and Ziliaskopoulos, T. (2003). A Decomposition Scheme for System Optimal Dynamic Traffic Assignment Models. Networks and Spatial Economics, 3(4):441–455.

Li, Z., Yu, H., Chen, X., Zhang, G., and Ma, D. (2019). Tsunami-induced traffic evacuation strategy optimization. Transportation Research Part D: Transport and Environment, 77(October):535–559.

Lighthill, M. J. and Whitham, G. B. (1955). On kinematic waves II. A theory of traffic flow on long crowded roads. Proceedings of the Royal Society of London. Series A. Mathematical and Physical Sciences, 229(1178):317–345.

Lim, G. J., Rungta, M., and Baharnemati, M. R. (2015). Reliability analysis of evacuation routes under capacity uncertainty of road links. IIE Transactions, 47(1):50–63.

Masucci, A. P., Smith, D., Crooks, A., and Batty, M. (2009). Random planar graphs and the London street network. European Physical Journal B, 71(2):259–271.

McGee, T. K. (2019). Preparedness and experiences of evacuees from the 2016 fort mcmurray horse river wildfire. Fire, 2(1):1–17.

Mohebifard, R. and Hajbabaie, A. (2019). Optimal network-level traffic signal control: A benders decomposition-based solution algorithm. Transportation Research Part B: Methodological, 121:252–274.

Moreno, A., Belanger, V., Cherkesly, M., and Rancourt, M.-E. (2023). Data set for evacuation network design and planning under traffic congestion. Mendeley Data, v1. Available at https://data.mendeley.com/preview/cptwg2r5bs?a=59e2598f-3690-41dd-8a40-7f9cdfe878c4.

Moreno, A., Munari, P., and Alem, D. (2019). A branch-and-Benders-cut algorithm for the Crew Scheduling and Routing Problem in road restoration. European Journal of Operational Research, 275(1):16–34.

Moreno, A., Munari, P., and Alem, D. (2020). Decomposition-based algorithms for the crew scheduling and routing problem in road restoration. Computers & Operations Research, 119:104935.

Murray-Tuite, P. and Wolshon, B. (2013). Evacuation transportation modeling: An overview of research, development, and practice. Transportation Research Part C: Emerging Technologies, 27:25–45.

Nafziger, J., Kovachis, N., and Emmer, S. (2021). A Tale of Two Basins: The 2020 river ice breakup in northern Alberta, part I: The Athabasca River. In 21st Workshop on the Hydraulics of Ice Covered Rivers, page 21.

Ng, M. W., Park, J., and Waller, S. T. (2010). A Hybrid Bilevel Model for the Optimal Shelter Assignment in Emergency Evacuations. Computer-Aided Civil and Infrastructure Engineering, 25(8):547–556.

Nunes, N., Roberson, K., and Zamudio, A. (2014). Comprehensive Guide for Planning Mass Evacuations in Natural Disasters. In The MEND Guide - Comprehensive Guide for Planning Mass Evacuations in Natural Disasters, page 116.

Rahmaniani, R., Crainic, T. G., Gendreau, M., and Rei, W. (2017). The Benders decomposition algorithm: A literature review. European Journal of Operational Research, 259(3):801–817.

Richards, P. I. (1956). Shock Waves on the Highway. Operations Research, 4(1):42–51.

Sherali, H. D., Carter, T. B., and Hobeika, A. G. (1991). A location-allocation model and algorithm for evacuation planning under hurricane/flood conditions. Transportation Research Part B: Methodological, 25(6):439–452.

Sheu, J.-B. and Pan, C. (2014). A method for designing centralized emergency supply network to respond to large-scale natural disasters. Transportation Research Part B: Methodological, 67:284–305.

Ulusan, A. and Ergun, O. (2018). Restoration of services in disrupted infrastructure systems: A network science approach. PLoS ONE, 13(2):1–33.

Üster, H., Wang, X., and Yates, J. T. (2018). Strategic evacuation network design (send) under cost and time considerations. Transportation Research Part B: Methodological, 107:124–145.

Waller, S. T. and Ziliaskopoulos, A. K. (2006). A combinatorial user optimal dynamic traffic assignment algorithm. Annals of Operations Research, 144(1):249–261.

White, R. A., Blumenberg, E., Brown, K. A., Contestabile, J. M., Haghani, A., Howitt, A. M., Lambert, T. C., Morrow, B. H., Setzer, M. H., Stanley, E. M., Velásquez, A., and Humphrey, N. P. (2008). The role of transit in emergency evacuation. In Transportation Research Board - Special Report, page 295.

Wolshon, B. (2001). "One-Way-Out": Contraflow Freeway Operation for Hurricane Evacuation. Natural Hazards Review, 2(3):105–112.

Wolshon, B., Catarella-Michel, A., and Lambert, L. (2006). Louisiana Highway Evacuation Plan for Hurricane Katrina: Proactive Management of a Regional Evacuation. Journal of Transportation Engineering, 132(1):1–10.

Wong, S., Shaheen, S., and Org, E. (2018). Understanding Evacuee Behavior: A Case Study of Hurricane Irma. In Transportation Sustainability Research Center, page 73.

Xu, J. and Nair, D. J. (2024). Explore the pre-disaster evacuation network design problem under five traffic equilibrium models. Computers & Industrial Engineering, page 110506.

Yan, X., Liu, X., and Song, Y. (2018). Optimizing evacuation efficiency under emergency with consideration of social fairness based on a cell transmission model. PLOS ONE, 13(11):e0207916.

Yao, T., Mandala, S. R., and Chung, B. D. (2009). Evacuation transportation planning under uncertainty: A robust optimization approach. Networks and Spatial Economics, 9(2):171–189.

Zheng, H. and Chiu, Y.-C. (2011). A Network Flow Algorithm for the Cell-Based Single-Destination System Optimal Dynamic Traffic Assignment Problem. Transportation Science, 45(1):121–137.

Zheng, H., Chiu, Y. C., and Mirchandani, P. B. (2015). On the system optimum dynamic traffic assignment and earliest arrival flow problems. Transportation Science, 49(1):13–27.

Ziliaskopoulos, A. K. (2000). A Linear Programming Model for the Single Destination System Optimum Dynamic Traffic Assignment Problem. Transportation Science, 34(1):37–49.